Industrialization of a micro-wind generation system

by

Carlos Lumbreras Iglesias

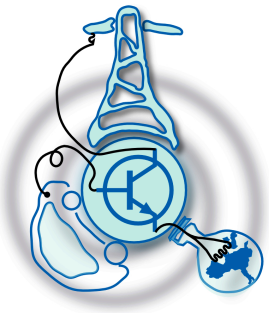

Submitted to the Department of Electrical Engineering, Electronics, Computers and Systems
in partial fulfillment of the requirements for the degree of

Master of Science in Electrical Energy Conversion and Power Systems

at the

UNIVERSIDAD DE OVIEDO

July 2013

© Universidad de Oviedo 2013. All rights reserved.

Author .....

Certified by .....
Juan Manuel Guerrero Muñoz
Associate Professor
Thesis Supervisor

Industrialization of a micro-wind generation system

by

Carlos Lumbreras Iglesias

Submitted to the Department of Electrical Engineering, Electronics, Computers and Systems
on July 22, 2013, in partial fulfillment of the
requirements for the degree of
Master of Science in Electrical Energy Conversion and Power Systems

Abstract

The project deals with the design of a small wind turbine generation system (< 2.5 kW) for single phase grid connection. The aim of this MTh is to develop the power electronics and control system needed for the proper operation of the wind turbine. This system must be efficient and totally autonomous since in its final stage it is intended to be commercialized by the company AZ Renovables, who financially supports this piece of research. In a previous project the selection of the power electronic topology and the basic control strategy for the power converter has been established. A demonstrator prototype was built to prove the main features of the system. This MTh will include new improvements in the control strategy (voltage and current control loops) needed to improve the system performance, allowing testing different MPPT algorithms. Since this electronic system is a part of a bigger electromechanical system, a full redesign of the PCB will be required in order to integrate it in the whole product. It will be also included in this MTh a wireless communication system to monitor the system main variables in real time. An important part of the MTh will be devoted to both study and meet the existing regulations in case of commercialization.

Thesis Supervisor: Juan Manuel Guerrero Muñoz
Title: Associate Professor

Contents

List of Figures

List of Tables

Chapter 1

Introduction

One approximation to micro wind turbines could be a small scale power generation system (up to 20 kW) which takes the energy from the wind although no clear regulation exactly define what micro wind turbines are. Usually these systems have a rotor area (or swept area) of less than 50 m^2. Is expected in the near future to set rules which clearly define which will be the limit of this technology to be considered as such.

Until now, these kind of systems were often used for standalone applications, supplying energy in places where there are no electric lines. Typically micro wind turbines were installed in vegetable patches, corrals, or cabins in the woods, but now this technology trends to be used for grid connected applications, for self consuming or power trading purposes.

Whatever is the purpose of the turbine, these are intended to be used in urban or industrial environments and consume its energy at buildings where it is produced or near them. These characteristics make micro-wind energy in a distributed energy production system, minimizing electrical losses in the energy transportation, preventing overloads in networks and the proliferation of large electric power plants.

1.1 Wind energy

The idea of using the energy of the wind as a power source is not new at all. This energy was used for at least 3000 years for grinding grain or pumping water. Also this energy was used for transportation in sailing ships.The firsts uses of windmills for electricity production can be found in the XIX century. Until our days, the technology of wind energy production has grown a lot, becoming nowadays in one of the most mature and developed renewable energy sources.

The power that is possible to capture with a wind turbine is given by the expression:

$$P = \frac{1}{2} C_p \rho A v^3 \tag{1.1}$$

where ρ is the air density (typically 1.2 $\frac{kg}{m^3}$), C_p is the performance coefficient of the wind turbine, A is the swept area by the rotor blades in m, and v is the wind speed in $\frac{m}{s}$.

C_p describes the fraction of the power in the wind that may be converted by the turbine into mechanical work, so power coefficient C_p will be responsible of the shape of the wind turbine power curves. This power coefficient depends on turbine characteristics and also depends on the tip speed ratio λ and the pitch angle β. This coefficient, as well as the tip speed ratio and the pitch angle, will be explained deeply in further chapters.

Broadly speaking, it can be said that the power that can be extracted from the wind is a cubic relationship with the wind speed. This is true when the system is operating at the maximum power point so it is important to provide the wind turbine with some algorithm allowing to track this maximum power point for all conditions, this being determinant when talking about the efficiency of the system.

1.2 State of the art

This Master Thesis can be considered as the second part of a previous work, where it was developed a digital control system for micro-wind energy [1]. There it was designed a system capable of handle a three phase permanent magnet generator and inject the extracted power into a single phase network. The rated power of this system is 2.5kW. This precedent project includes the power electronics topology selection, the design of the electronic circuits needed for the proper working of the system which includes control system (DSP), sensors, IGBT firing circuits and all rest of auxiliary components such as power supplies, communications or protections.

Also in that previous work there were defined some control strategies that allow the system to control the power from the turbine as well as the software needed to implement all control loops in a DSP.

At the end of previous project there were achieved the next points:

- A valid power electronics topology selection
- A valid hardware prototype for power injection
- Correct grid synchronization
- Unity power factor
- A valid control strategy for a fixed generator speed

1.3 Objectives of the Master Thesis

The goal of the present Master Thesis is to improve the previous system in such a way the system can work autonomous, allowing to create a commercial product as much efficient as it cans sharing a high degree of efficiency.

In this MTh will be presented all improvements considered in hardware components, including electronic schemes and a fully redesign of the PCB needed to integrate it within the turbine nacelle.

Concerning to the control strategy, this will be modified to achieve a smooth control in all current and voltage conditions. This new control strategy must allow the system to request a constant power to the generator and inject it into a single phase network. Also the control strategy must provide to the system the ability of implementing Maximum Power Point Tracking algorithms (MPPTs), increasing the efficiency of the system as much as possible.

It is also the aim of this Master Thesis there to provide the system with a wireless communication system to monitor the system variables, including a client application for PC to display them.

All the electrical systems and the improvements included in the present MTh must be compliant with the actual existing regulations that allow the product to be commercialized, so an important part of this MTh will be the studying and meeting of these regulations.

Chapter 2

Hardware

This chapter will include the modifications performed in the electronic schemes to achieve a reliable, robust and flexible system. This chapter will also show the redesign of the PCB, needed to integrate it in a commercial product.

Previous schematic design include all components needed for a basic working system. This includes power sources, IGBT drivers, sensors, and power electronics topologies. The system described depended on an external PCB for the DSP connection (TMS320F28335 Experimenter Kit) and previous current sensors did not work properly. Besides, there were some isolation problems between the DSP and the USB connection of the PC, which required to include an external USB isolation system to prevent short circuits since the ground signal of the USB was earthed.

Although the former system was correctly working, there were some components that were very tight for the application, and in order to improve the reliability of the system some of them were substituted by other more reliable. Moreover some components were added in order to improve the characteristics of the system as it can be the PWM output where a current buffer was added.

In the previous design, the only point that was not correctly working was the power supply, making the system dependent on an external one. In this review, all issues concerning power supplies were successfully solved, being all components integrated in the same PCB and independent of external devices.

In Fig. 2-1 it can be seen a picture of the previous PCB. In the picture, it can be

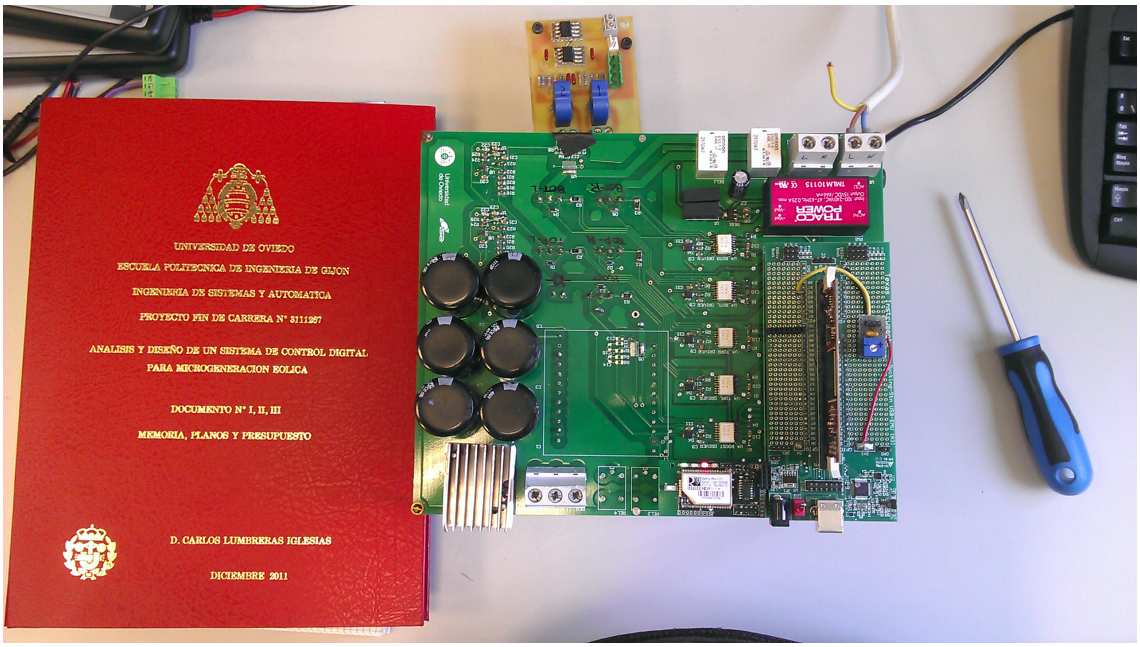

Figure 2-1: Previous version of the system

appreciated the external current sensors, the board for mounting the DSP and the high number of capacitors used.

2.1 Design improvements

This section decribes all improvements done in the electronic schemes. This includes the integration of the DSP in the system, inclusion of PWM current buffers, new power sources, reduced number of capacitors, new current sensors, and other minor improvements.

2.1.1 DSP integration and USB isolation circuit

One of the problems found facing a future commercialization of the generating system is the dependance on an external PBC (Printed Circuit Board) as is TMS320F28335 Experimenter Kit. To avoid this dependance, DSP will be integrated in the main PCB. To do this, it will be necessary to include both all the DSP connections with the rest of the components (sensor, drivers..) and the communication part between

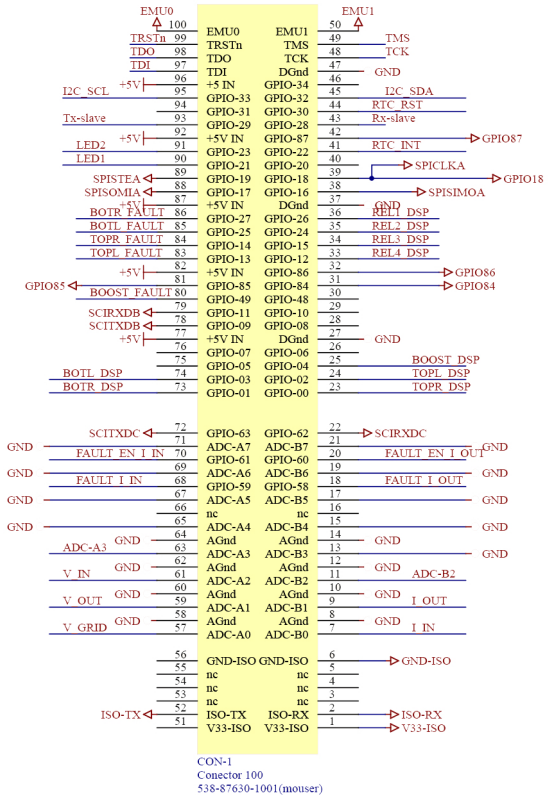

Figure 2-2: DSP 100 pin connector

the DPS and the USB PC connection.

The connection between the main board and the DSP will be through a 100 pin connector. This connector will provide access to the main I/O pins of the controller, among them are included PWM signals, several GPIOs, Analog to Digital channels and RS232 port. Through this connector will be also wired the FTDI and the circuitry needed for the DSP USB programming. In Fig. 2-2 it can be seen the interface between DSP and all the external connections.

For the connection of the DSP and the PC it is needed to add a FTDI chip, which allows to communicate the DSP with a USB system through the UART port. The scheme for this circuit was taken from those provided by the manufacturer Texas Instruments. In order to obtain galvanic isolation between the PCB and the UBS connection, an ADUM4160BRIZ IC will be used. This is a specific component used to provide galvanic isolation in USB connections. The component isolates data line of the serial bus, avoiding current flowing between the PCB and the PC. This isolation is

needed since the USB GND signal is earthed so this can cause short circuits between the system and one line of the grid.

Including these communication components it is possible to remain safety while the DSP and PC are connected for debugging and programming purposes.

2.1.2 PWM buffer

This generation system is thought to be controlled by semiconductor devices. These devices need to be controlled in order to properly work. The way that the system is going to be controlled is through Pulse With Modulation (PWM) and in order to control the PWM accurately, PWM module of the DSP will be used.

In the previous design, the DSP PWM outputs were directly attached to the drivers of the IGBT. This means that the DSP must provide all the current that the driver request in order to turn on and off its internal optocouplers. The DSP can supply or accept currents up to 8 mA through PWM pins while the minimum current to guarantee the turn on of the optocouplers is also 8 mA. With these numbers all looks to be fine but the components were very tight and some parasitic resistance due to aging of the components can make the system fail.

In order to improve this issue and avoid this situation, it has been include a current buffer. This will also be needed in case of replacing the driver for another one which could require more current, providing flexibility and reliability to the system.

The buffer selected is a SN74LVC2244APW IC from Texas Instruments. This is a non-inverting octal buffer which is able to handle up to 12 mA in both directions. This fits better with the characteristics of the driver and allow to the PWM module working in low consumption mode enlarging the life of the system.

From the eight signals available in the buffer only five will be used. Four of this signals are used to drive the inverter and the remaining one is used to drive the boost converter. The other three signals will not be used, being available for future uses.

2.1.3 Power sources

One of the previous design problems were the auxiliary power sources. In the previous design, it was used a main power source consistent on an AC/DC converter. This power source was directly connected to the grid providing an output voltage of 15 V which was needed for directly supplying the IGBT drivers. The 15 V rail was converted to 5 V through a linear regulator which was used to supply the DSP, relays, and current sensors. A 3.3 V rail needed for voltage sensors and other ancillary components was obtained from 5V by using another linear regulator.

This cascaded topology did not work properly because the 5 V regulator required a high amount of current from the 15V power source and got hot very fast, causing malfunctions in the regulated voltage. This issue was solved in the previous version using an external power source, becoming the system dependent of external components which was acceptale for debugging purposes but prevents from autonomous operation.

In order to solve this problem, the 15 V main power supply was replaced by a 5 V one. The 15 V rail needed for firing IGBTs are now obtained from isolated DC/DC converters (5 V - 15 V). The 3.3 V rail is adapted from the main power supply using a linear regulator. This solution avoids the heating observed problem in the 5 V linear regulator, since the 5 V is the most overloaded one due to the relatively high consumption of the DSP, relays and current sensors with respect to other components.

With this solution it is possible to maintain the number of power sources, the size, and the cost of power supplies. It must be noted that in previous circuit isolated 15 V-15 V DC/DC converters were also needed for firing the IGBTs.

2.1.4 Redistribution of capacitors

One of the improvements in this schematic review is the redistribution of the capacitors. In previous version there were a lot of capacitance available at the rectifier output with a comparatively small one in the DC-link. However, it can be demonstrated that a higher value of capacitance in the output of the rectifier impoverish

the power factor in the generator side.

This can be solved by reducing the rectifier output capacitance , decreasing the number of capacitors used (and thus the price) and improving the power factor in the generator side.

The new value for this capacitance can be calculated from the admissible voltage taking into account maximum current ripple in the current though the boost converter.

As it was defined in the previous version of this work, maximum current ripple in the boost inductor is 1A peak-to-peak and the maximum admissible voltage ripple in the capacitors is 5V.

The voltage ripple in a capacitor through which flows an AC current can be calculated as (2.1):

$$C = \frac{Q(t)}{V(t)} \quad \rightarrow \quad \Delta V = \frac{\Delta Q}{C} \tag{2.1}$$

where C is the capacitance value, Q is the charge is the capacitors and V is voltage. The charge due an AC current in a capacitor can be expressed as 2.2:

$$\Delta Q = \frac{1}{2}\frac{\Delta i_{AC}}{2}\frac{T}{2} \quad \rightarrow \quad V_{pp} = \frac{\Delta Q}{C} = \frac{\Delta i_{AC}}{8\ f\ C} \tag{2.2}$$

from 2.1 and 2.2 can be obtained the value of a capacitor through the AC current and the maximum admissible voltage ripple as can be seen in 2.3

$$C = \frac{\Delta i_{AC}}{8\ f\ V_{pp}} = \frac{1A}{8\ 20000Hz\ 5V} = 1.25\mu F \tag{2.3}$$

2.1.5 Current sensors

One of the main problems in the previous design were the current sensors. Those sensors were Allegro ACS709 ICs. They are coreless Hall effect current sensors. The fact of not having core makes them very sensitive to external magnetic fields so the output of these sensors can be easily distorted if they are placed near a magnetic field source.

Other problem detected with this sensors was the low common mode voltage supported by them. They can be easily damaged when they are used in voltage lines above 320V.

The solution adopted for the current sensors was to replace them with a sensor which can handle high common mode voltages. This sensor is the LTS15 from LEM. It is a closed-loop Hall effect current sensor with unipolar voltage supply. It can measure up to ± 15A AC current accurately providing a voltage output.

In order to improve the signal integrity after the AD conversion, an anti-aliasing filter will be added.

2.1.6 Other minor improvements

Apart of the mentioned improvements, which can severely affect to the control and behavior of the system, there are also included in the circuit other minor changes that provide more functionalities and flexibility to the system.

- Two Analog-to-Digital channels are available for additional measurements such as temperature sensors placed in the stator winding of the generator, or close to the IGBTs.
- Two LEDs are now included in the circuit for visual inspection. This can be useful to know the state of the system in every moment with a peek. Also a buffer was included to properly drive these LEDs.
- A Real Time Clock (RTC) was included over the I^2C communication bus. This will be used to store in a memory relevant events as can be alarms.
- A EEPROM memory over I^2C to store relevant events.
- A battery was included, with its own battery charger, to keep the time data in the RTC.
- All communication buses are accessible for possible future expansions as well as the boot resistors for flash operation of the DSP.

Real Time Clock

An RTC was included to know when a relevant event occurs and store it in memory. The RTC selected is DS3232 from Maxim IC. This clock can count seconds, minutes, hours, days, months, and years (with leap year compensation).

Also this device has the possibility to create elapsed alarms which can be useful for periodic routines as can be communications with a remote server.

This component can work over a I^2C bidirectional bus with a clock frequency up to 400kHz. The address of this device is 0x68. DS3232 also has embedded a temperature sensor and a small SRAM memory than could be useful to store configurations or some relevant data.

To avoid the loss of the stored data or the date, it is needed to add a small battery to keep the RTC working when the system is not connected, avoiding having to update the device every time the system is switched on.

EEPROM memory mapping

An EEPROM memory will be also added to the main circuit. This memory is useful to store relevant events such as alarms or to store data relative to the energy produced for monitoring purposes. The selected memory is 24AA1026 from Microchip. This is an I^2C device with 131072 memory positions. The slave address for this component can be easily selected with 4 pins available.

This memory will be splitted in two parts, one part for fail messages history and the other for data storage.

Each error message will be composed of 7 bytes (Table 2.1) and is possible to store up to 9216 error messages.

For power data storage, the structure is more or less the same. It is though to be stored in the memory the average value of the power injected each minute. The length of a single power data is 6 bytes (Table 2.2).

Error memory will be distributed as it is shown in Table 2.3. In this mapping it is included the total number of errors stored in the memory (two bytes) and the last

YEAR
MONTH
DAY
HOUR
MINUTE
SECOND
ERROR

Table 2.1: Fail message storage structure

YEAR
MONTH
DAY
HOUR
MINUTE
PWR DATA

Table 2.2: Alternative fail message storage structure

error read (two bytes).

A pointer to a specific error is easily calculated by (2.4) and (2.5).

$$Page = \frac{Errornum. - 1}{36} \tag{2.4}$$

$$Pointer = (Errornum. - 1)\%36 + 4 \tag{2.5}$$

For the power data storing the mapping structure is the same (see Table 2.4). A pointer to a specific data position is easily calculated by (2.6) and (2.7).

$$Page = \frac{Errornum. - 1}{42} \tag{2.6}$$

$$Pointer = (Errornum. - 1)\%42 + 4 \tag{2.7}$$

0x0000	Num. Error H	0x0100	-
0x0001	Num. Error L	0x0101	-
0x0002	Last Error H	0x0102	-
0x0003	Last Error L	0x0103	-
0x0004 : 0x000A	ERROR 1	0x0104 : 0x010A	ERROR 37
0x000B : 0x0011	ERROR 2	0x010B : 0x0111	ERROR 38
: : :	: : :	: : :	: : :
0x00F9		0x01F9	
:	ERROR 36	:	ERROR 72
0x00FF		0x01FF	

Table 2.3: Error message mapping

0x0000	Num. Data H	0x0100	-
0x0001	Num. Data L	0x0101	-
0x0002	Last Data H	0x0102	-
0x0003	Last Data L	0x0103	-
0x0004 : 0x0009	DATA 1	0x0104 : 0x0109	DATA 43
0x000A : 0x000F	DATA 2	0x010A : 0x010F	DATA 38
: : :	: : :	: : :	: : :
0x00FA		0x01FA	
:	DATA 42	:	ERROR 84
0x00FF		0x01FF	

Table 2.4: Data message mapping

2.2 PCB redesign

Previous PCB shape was a square good for testing the behavior of the components, but besides some errors and the commented improvements its shape was not suitable for the product integration. All the electronics used for control the system must be integrated inside the generator case. It has been planned to be mounted behind the generator, inside the nacelle. This is why the PCB must have a certain of circular shape. A sketch of the final shape can be seen in Fig. 2-3.

The flat zone on the top is for cooling issues. The IGBTs will be attached to the turbine frame, that will serve as spendthrift. The PCB will have a hole in the center that will serve for cooling since a fan will be attached to the generator shaft. The lower in the PCB is to place the brushes needed to allow the turbine to turn, facing the wind in any direction like a wind vane. The PCB will also include some guidelines and small holes for assembly purposes.

The mechanical drawings were designed in collaboration with the company that is funding this project. In Fig. 2-4 it can be seen a picture of a mounted PCB.

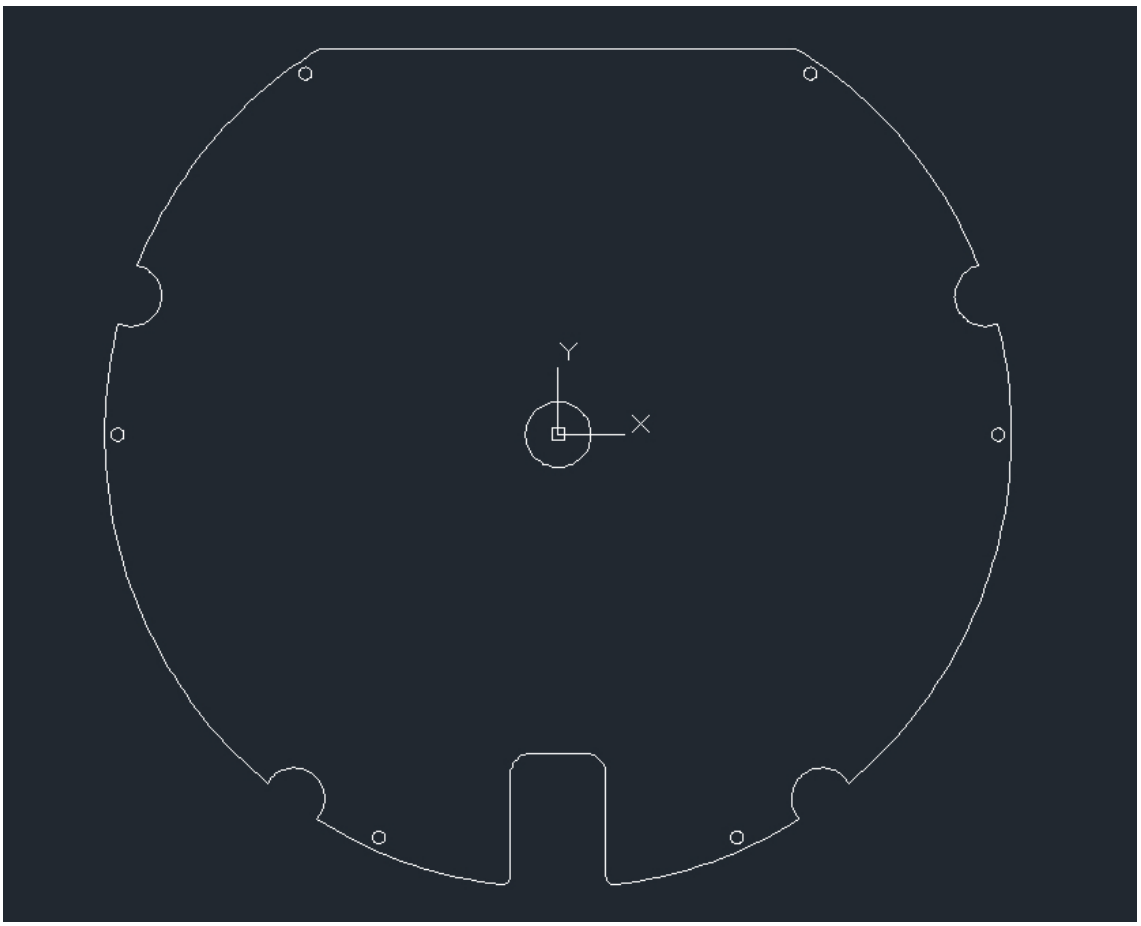

Figure 2-3: PCB Skecth Shape

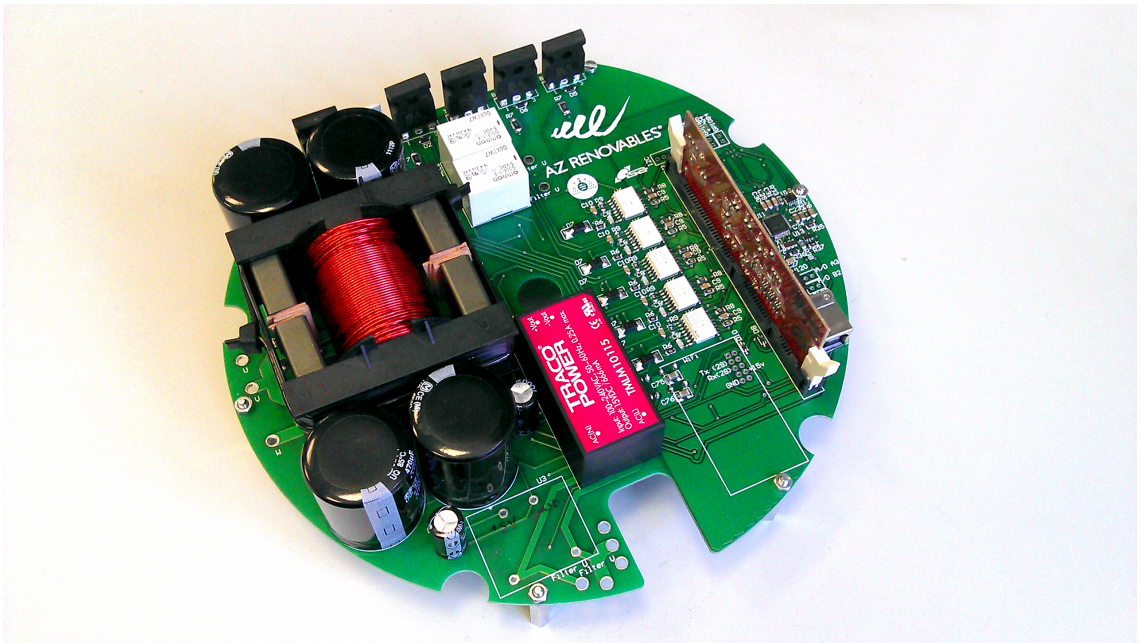

Figure 2-4: Photo of the built PCB

Chapter 3

Model and simulation of a wind turbine

As it was introduced in previous chapters, a wind turbine is a machine that converts the linear movement of the wind into a rotational movement of the rotor of the turbine. An electric generator is connected to the rotor shaft and when the wind blows, the rotor turns and the generator produces electricity.

The maximum power that is possible to capture from the wind follows a cubic relation with the wind speed. According to (3.1) the power that the turbine is able to capture depends on the fluid density ρ (typically air 1.2 $\frac{kg}{m^3}$) and the size of the turbine. The larger the turbine, the higher the power that is able to capture.

$$P(t) = \frac{1}{2}\pi r^2 \rho v(t)^3 \tag{3.1}$$

According to Betz's law, a turbine can not capture more than 16/27 (59.3 %) of the kinetic energy in wind [5]. This value is known as Betz's coefficient and is the highest performance that a wind turbine can reach. It dates from 1920s. The basic principle used to obtain this value states that the fluid flow remains rectilinear when passing through the turbine and maintains a uniform distribution of the fluid pressure on the turbine. This is a simplification and some aspects as can be the blades aerodynamic resistance are not taken intro account, so a more accurate value for this

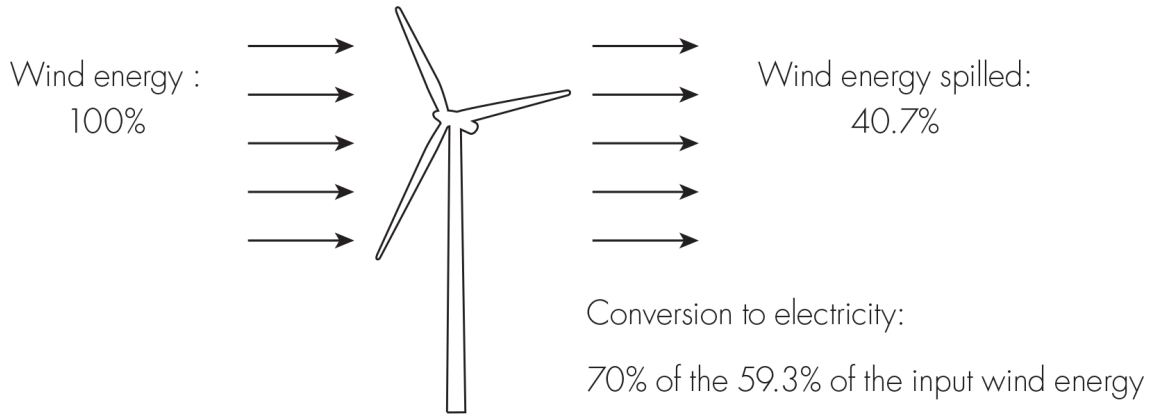

Figure 3-1: Air flowing through the turbine

limit will be lower.

This limit considers that if all the energy of the wind that is ingoing to the turbine is taken, there will be no air flow through the turbine. This is because the energy available from the wind is kinetic energy. If all the energy is taken from the wind, there would be not kinetic energy and because of this the wind speed would be 0. If the wind speed after the turbine is 0 there will be no room for more air and is not possible to capture more energy. In order to keep the wind moving the outgoing air has to have some movement (Fig. 3-1). Betz' law shows that as air flows through area, and when it slows from losing energy to extraction from a turbine, it must spread out to a wider area. Geometry is what limits the turbine efficiency to 59.3%.

According to this limit the power that is possible to capture from the wind is limited by the wind turbine performance, that has to be always lower than the Betz's limit (3.2). This performance, also called rotor power coefficient C_p is not a fixed parameter. This parameter varies depending on the mechanical characteristics of the turbine, and also depends on the actual tip speed ratio λ and the pitch angle β.

$$P = \frac{1}{2}\pi r^2 \rho C_p(\lambda, \beta) v^3 \tag{3.2}$$

The tip speed ratio can be defined as the relation between the linear speed or the tip of the blade and the wind speed (3.3). In this case and almost in all small scale wind turbines, the pitch angle is fixed, so for this specific turbine this angle will be

Diameter	1.75 m
Nominal Wind Speed	12 $\frac{m}{s}$
Nominal rotational speed	600 rpm
Nominal Power	1185 W
Air density	1.2 $\frac{kg}{m^3}$

Table 3.1: Wind turbine parameters

zero $\beta = 0$.

$$\lambda(t) = \frac{\omega(t)R}{v(t)} \tag{3.3}$$

The wind turbine to be modeled has the parameters shown in table 3.1

3.1 C_p estimation

A goop estimation of this coefficient is very difficult to obtain. This parameter is normally obtained from the power curves of the turbine empirically obtained.

From this curves it can be obtained a mathematical model which behavior is quite similar to the actual one. This mathematical model is a largely discussed issue and there can be found several valid options. This is explained in more detail in [6] - [9]. In this case it will be used the model that appears in [10].

Power coefficient is a function of the tip speed ratio λ and the pitch angle β. From the curves obtained by testing wind turbine it can be obtained the maximum value for this coefficient. The value for different wind speeds and rotational speeds can be calculated by using mathematical approximations by using the expression (3.4).

$$C_p(\lambda, \beta) = c_1(\frac{c_2}{\lambda_i} - c_3\beta - c_4)e^{\frac{-c_5}{\lambda_i}} + c_6\lambda \tag{3.4}$$

with

$$\frac{1}{\lambda_i} = \frac{1}{\lambda + 0.08\beta} - \frac{0.035}{\beta^3 + 1} \tag{3.5}$$

where coefficients $c_{1..6}$ depend on mechanical characteristics of the turbine.

c_2	200
c_4	11
c_5	7.5

Table 3.2: Wind turbine c coefficients

In this particular case, expressions (3.4) and (3.5) can be simplified since the pitch angle of the blades are 0. Simplified expressions are (3.6) and (3.7).

$$C_p(\lambda) = c_1 \left(\frac{c_2}{\lambda_i} - c_4 \right) e^{\frac{-c_5}{\lambda_i}} + c_6 \lambda \tag{3.6}$$

with

$$\frac{1}{\lambda_i} = \frac{1}{\lambda} - 0.035 \tag{3.7}$$

where c coefficients that fit with the turbine to be modeled are in Table 3.2.

The rest of parameters can be obtained from the parameters of tables 3.2 and 3.1.

$$\lambda_{rated} = \frac{\omega_{r_{rated}} R}{v_{rated}} \tag{3.8}$$

$$C_{p_{max}} = \frac{2P_{rated}}{\rho A v^3} \tag{3.9}$$

$$\lambda_{i_{rated}} = \frac{1}{\frac{1}{\lambda_{rated}} - 0 - 035} \tag{3.10}$$

$$K_{rated} = \frac{(-\frac{c_2 c_5}{\lambda_{i_{rated}}} - c_4 c_5 - c_2) e^{\frac{-c_5}{\lambda_{i_{rated}}}}}{\lambda_{rated}^2} \tag{3.11}$$

$$c_1 = \frac{C_{p_{max}}}{\frac{c_2}{\lambda_{i_{rated}} - c_4} e^{\frac{-c_5}{\lambda_{i_{rated}}}} + K_{rated} \lambda_{rated}} \tag{3.12}$$

$$c_6 = K_{rated} c_1 \tag{3.13}$$

With these coefficients it is possible to numerically obtain the curves of the turbine,

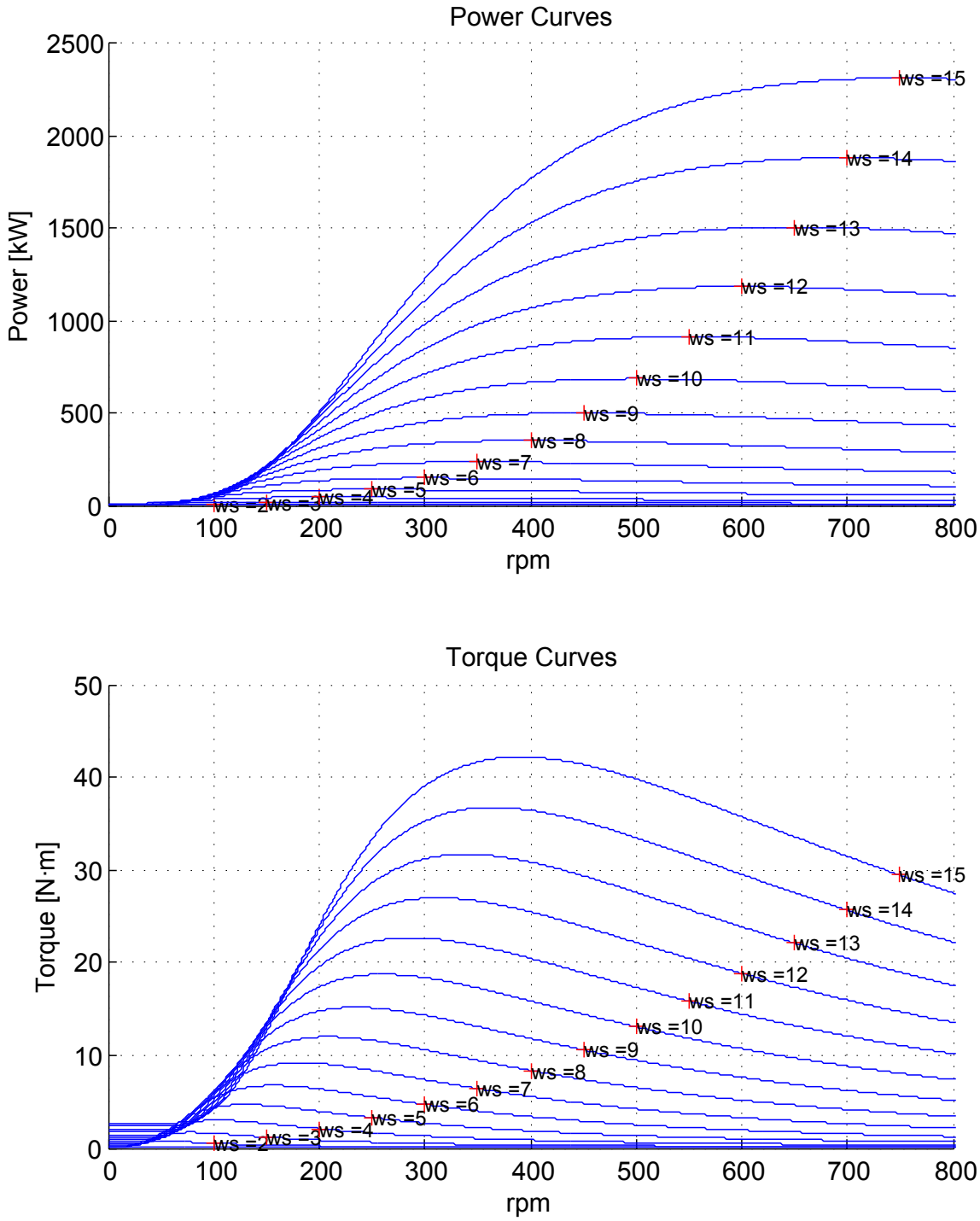

Figure 3-2: Power and torque curves obtained with the model of the wind turbine as a function of the angular speed and the wind speed

Num. poles	12 Ω
Magnets constant	833 $\frac{V_{pk}}{krpm}$
Rs	6.67 Ω
Ls	0.074 H

Table 3.3: Parameters of the generator AZR / PMG-01

Rated power	11kW
Num. poles	4 Ω
Voltage	380Y
Frequency	50Hz
Rated speed	1465rpm
Current	23.70
cos ϕ	0.82

Table 3.4: Parameters of the induction motor used to simulate the turbine

which will be used to simulate its behavior. In Fig. 3-2 it can be seen the power and torque curves of the wind turbine for wind speeds from 1 to 15 m/s. The maximum power points are marked with a '+'.

3.2 Wind Turbine Simulation

In order to have a platform for testing the generator independently of the climatic conditions, the wind turbine of table 3.1 has been simulated by using the equations explained in previous section, where the input of the model is the wind speed.

For this purpose an induction motor will be coupled with the generator of the system. In this case, the induction motor will be controlled by a frequency converter in order to behave as a real wind turbine, simulating the behavior of the turbine shaft as a function of the wind speed.

The generator used has been built and designed by 'AZ Renovables' specifically for this application. The parameters of this generator can be seen in table 3.3. The asynchronous machine used to simulate the turbine behavior is an ABB 11 kW machine which parameters are shown in table 3.4.

The wind turbine will be simulated with the induction motor by using a commercial inverter. This converter will be configured in closed loop torque control in which

the torque command will be obtained by substituting the result of (3.2) in (3.14). The rotor speed will be obtained through an encoder attached to the motor shaft.

$$T = \frac{P}{\omega} \tag{3.14}$$

The frequency converter used to control the induction motor is a *SP2403* from *Control Techniques*. The module used to program the calculations needed for the torque command is *SM Application Lite*. This way it is possible to create a program to calculate the torque command with a small processing time.

The wind speed to be simulated can be introduced to the program any time. This will be introduced manually through the watch window of the program. A screen snapshot of this interface ca be seen in Fig. 3-3. In Fig. 3-4 it is shown the generator attached to the induction machine.

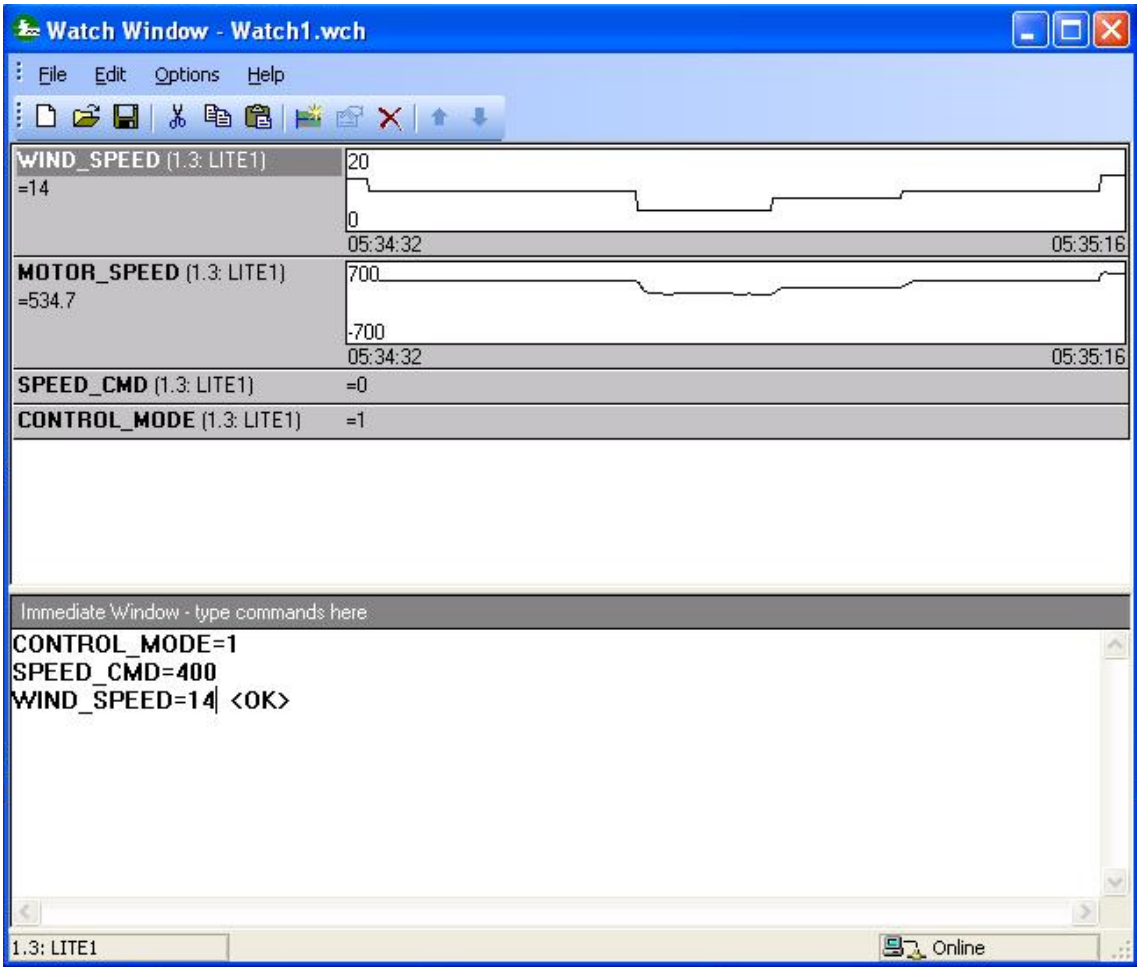

Figure 3-3: Snapshot of the wind turbine simulator

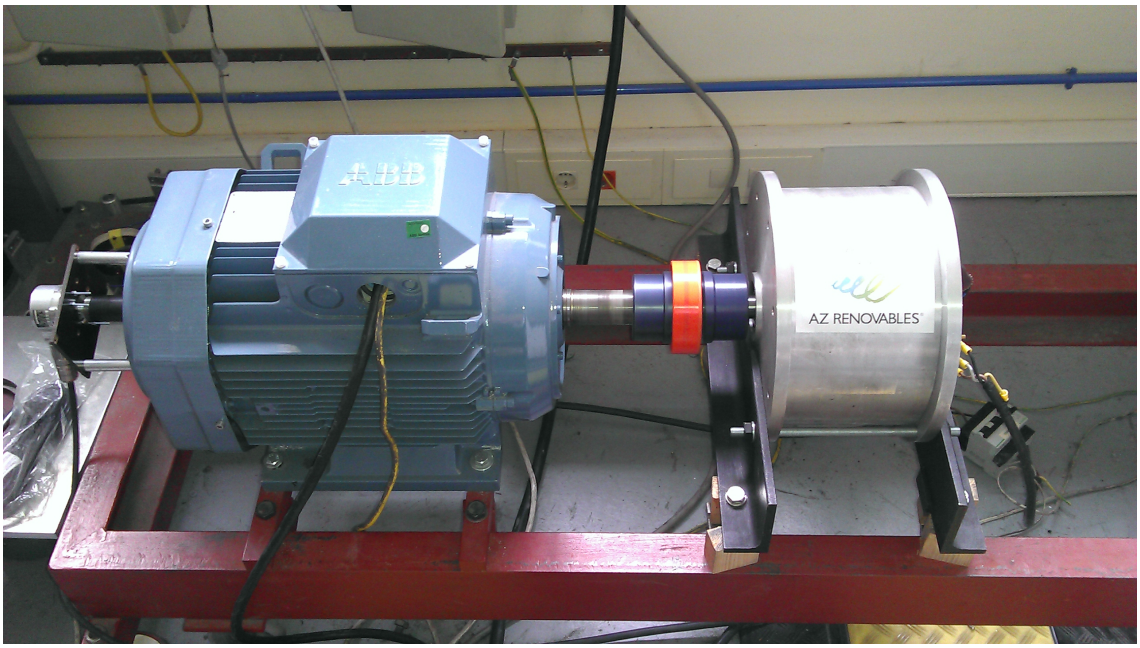

Figure 3-4: Photo of the wind turbine simulator

Chapter 4

Control

This chapter will present all modifications and additions related with the control strategy. In the previous project it was introduced a simplified control strategy that allowed to inject power into the grid but making hard to control the power required from the generator side.

In that previous control system the, boost converter was used to control the DC bus voltage, keeping it to a constant value, with no oscillations. The inverter controller was the responsible of the current injected in the grid. The power extracted from the generator was controlled by modifying the injected current command without implementing any maximum power point tracking algorithm.

One problem of that control strategy is that the power injected in a single phase system cannot be constant while in a three phase generator the power is constant. With the previous strategy, instantaneous power variations produced because of the power injected to the grid were directly transmitted to the generator producing the subsequent torque fluctuations in the turbine. As the grid has a constant frequency, this power variation is fixed to the double of this frequency (typically 100 Hz for European networks) and this fluctuation will be transferred to the generator which will cause a torque pulsation of 100 Hz in the wind turbine.

Also, there were found some improvements that can be done in the synchronization process. The algorithm that was used in the previous work obtain the phase of the single phase waveform by measuring the grid voltage and calculating its phase as

the arc-tangent of the α β components of this voltage were the β component is calculated as the derivative of the grid voltage. The synchronization was reached perfectly but computationally it takes a lot of time due the arc-tangent method that was implemented before. Also, the previous method was dependent on a band pass filter that need retuning when connecting the system to a non European network (50 Hz). Apart from this, the frequency and voltage magnitude cannot be obtained directly with the arc-tangent method making necessary to separately calculate those parameters. It is worth to mention that both parameters, network frequency and voltage magnitudes, are requested to comply with regulation issues as can be the islanding operation or voltage supporting.

In this chapter they will be presented new methods and a new control strategy to provide solutions to previous problems plus new improvements that allow to handle the system safely under high wind speeds.

4.1 Grid synchronization method (PLL)

Many regulations concern frequency network and voltage magnitude issues, mainly those related with islanding operation modes or voltage support. The method used in the previous work, achieved grid synchronization with an arc-tangent calculation that do not provide those two parameters.

Other disadvantage of the previous method is its dependency on a fixed band pass filter prevent it from working in different frequency networks.

Grid synchronization is a very important issue because this stage will be critical to obtain an unity power factor. This is why it is important to synchronize well in all possible networks (50Hz and 60Hz).

One method that can solve these issues is a PLL which can be synchronized with 50Hz and 60Hz power networks without band-pass filters. This method also provides the information of frequency and voltage level needed to comply with regulations. A Phase-Locked-Loop (PLL) is an estimator that generates an output signal whose phase is related to the phase of an input signal. This mechanism can be implemented

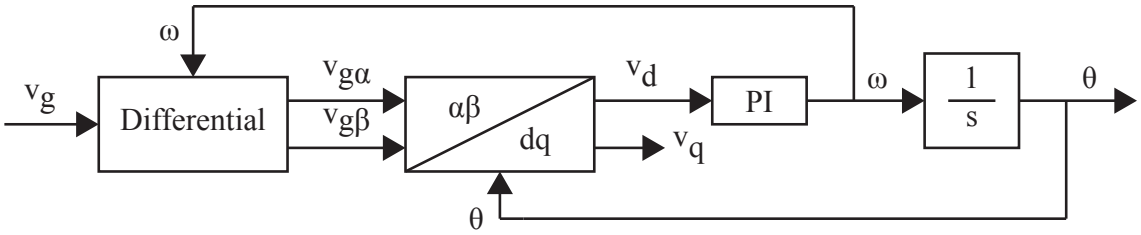

Figure 4-1: Block diagram for PLL synchronization method.

in a DSP and can be used as grid phase detector for a unity power factor.

One of the main problems in single phase networks for PLL implementation is the availability of only one signal. This problem can be partially solved obtaining a second signal in quadrature with the original. This second signal can be obtained by differentiation of the original signal since this is a sinusoidal wave. The main disadvantage of this method is that the resultant waveform is very noisy and its dependent of the actual frequency that is one of the unknowns.

As PLL is a closed loop method, grid frequency can be obtained for the differential and angle calculation. Once the quadrature signal has been calculated, it can be applied the Park transform and a synchronous PLL [11] and [12]. Synchronous PLL takes advantage of the synchronous reference frame obtained from Park's transformation and synchronizes with q-axis signal in such a way the d-axis variable is used as the error signal. When v_d becomes 0 means the system is synchronized with the grid, being ω_e the grid frequency, θ_e the phase and v_q the amplitude of the grid voltage. A block diagram showing the implementation of method can be seen in Fig. 4-1.

The PI controller was calculated for a bandwidth of 100 Hz. The resultant controller can be seen in (4.1).

$$\frac{\omega_e}{v_{g_d}} = 1.73\frac{s + 57.8035}{s} \quad \left[\frac{\frac{rad}{s}}{V}\right] \tag{4.1}$$

4.1.1 Simulation results

This method was tested by simulations using MATLAB. The input signal will be a sinusoidal wave of 230 V rms and 50 Hz during the first 0.25 s and after this time

it is changed to 110 V and 60 Hz in order to test the of synchronization ability with two different systems. In order to make the simulation as much realistic as possible, a random white noise of as much ± 10 V have been added to the main signal which is higher from what is generally present in the DSP measurement after AD conversion. This noise can be found in the actual system both in the output of the AC voltage sensor and in the ADC conversion in the DSP.

As the PLL method uses the frequency calculated ω_e to calculate the quadrature signal, this frequency has to be initialized. For this case the initial frequency will be 1 Hz in order to test the dynamic response of the method.

In Fig. 4-2 there are shown the results of the PLL. In the upper part it is shown the grid voltage in blue v_{g_α} and in red the quadrature signal v_{g_β}. This signal is very noisy due to the random noise added to the original signal, which more or less is what it can be found in a real system. In the middle-up part of the figure it can be seen the estimated frequency which response is very fast and allows to detect frequency changes quickly enough (less than three cycles). In the low part of the figure it can be seen the phase of the original signal calculated with PLL method. The estimated amplitude can be seen in the low part of the figure where $V_{g_d}^e$ (in blue) is the error signal used for the synchronization that in steady state must be 0 and $V_{g_q}^e$ (in red) is the estimated amplitude of the grid voltage.

In order to test how accurate are the values obtained with the PLL, in Fig. 4-3 it is shown a comparison between the original signal (in blue) and the one built from the PLL data (in red). In the low part of this figure it is shown the error between both signals that in steady state is of $\pm 15V$ for 50 Hz signal and ±10 for 60 Hz signal which compared with noise added to the original signal (± 10 V) is a quite good result.

4.2 Control strategy

The previous control strategy adopted was split in two different control loops, one for the boost converter and one from the inverter control. The boost converter control

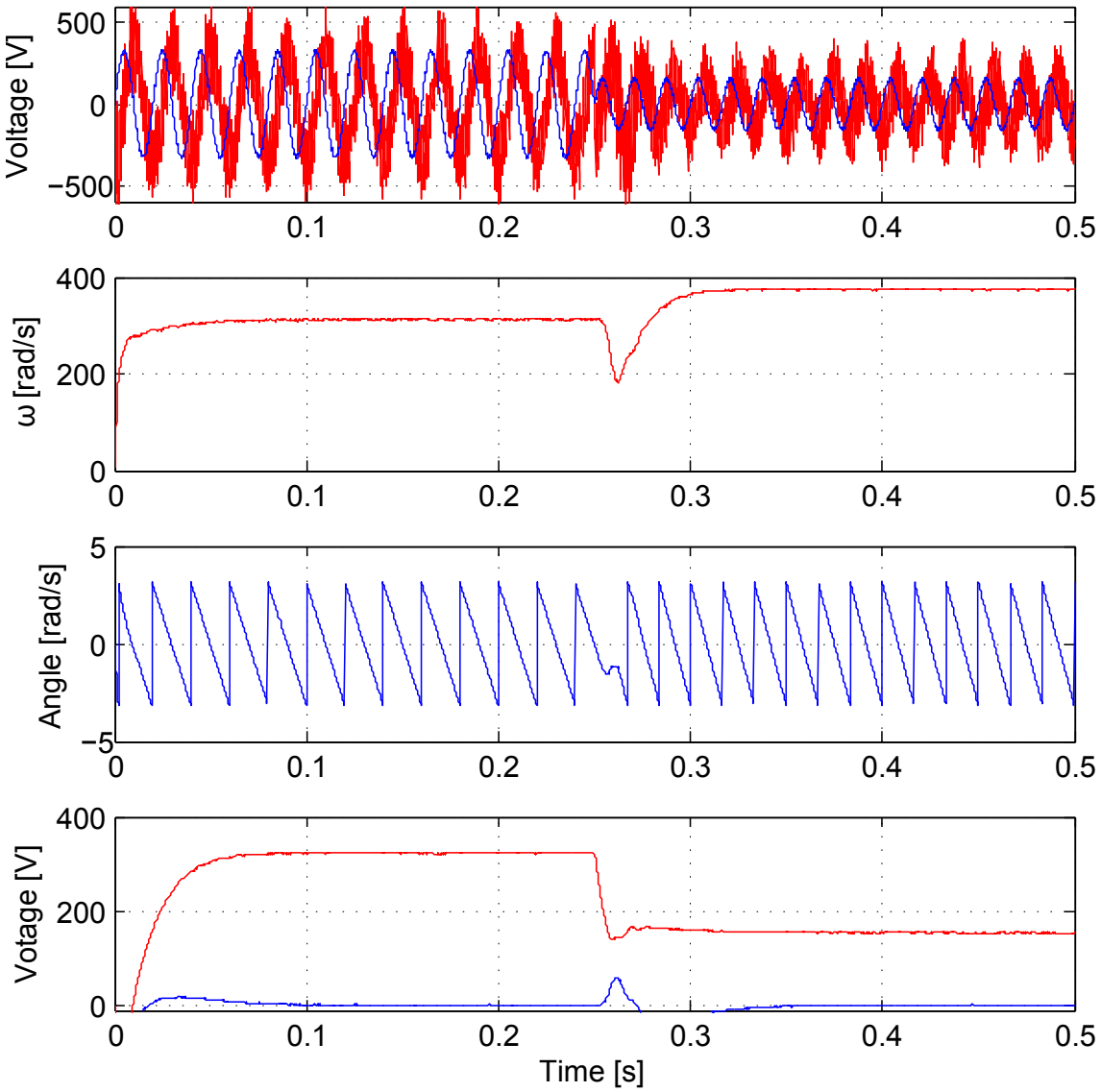

Figure 4-2: PLL results.

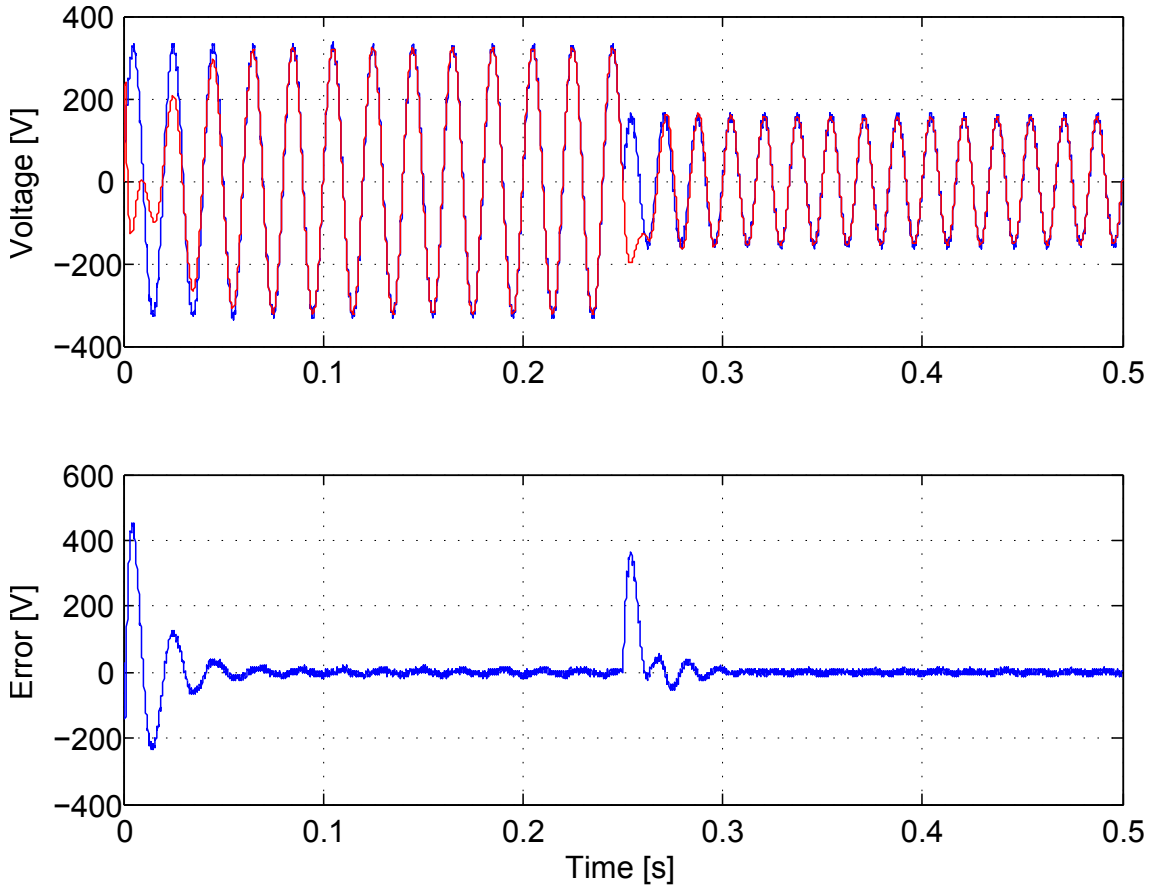

Figure 4-3: Comparison between original signal and the one obtained with PLL results.

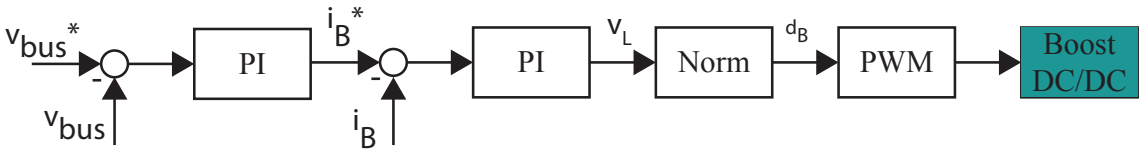

Figure 4-4: Blocks diagram of previous control strategy: Boost converter.

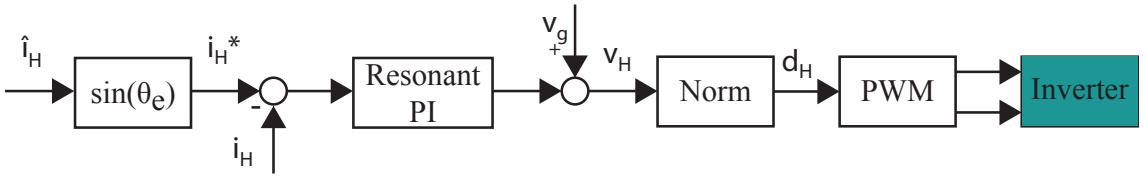

Figure 4-5: Blocks diagram of previous control strategy: Inverter.

loop was in charge of controlling the DC-link voltage level to a constant value, while the inverter control loop was in charge of controlling the sinusoidal injected current with a unity power factor.

The boost converter controller had two cascaded control loops, one for voltage and one for current. The inner control loop was in charge of controlling the boost current (i_B). The reference for this i_B current was provided by the voltage outer loop, that was in charge to control the DC-link voltage (v_{bus}) to a constant value. Block diagrams for these control loops can be found in Fig. 4-4.

The inverter controller was a single control loop which command signal is the amplitude of the desired injected current. The instantaneous value for this current is calculated by using the grid voltage phase, calculated previously with the arc-tangent synchronization method. Once the instantaneous value has been calculated, it was applied a resonant PI regulator in order to inject current in phase with the grid voltage. In order to improve the dynamics of the resonant controller, a grid voltage feed-forward term V_g was included, avoiding distortions by this voltage at the start-up of the control, improving the behavior of the regulator. This control scheme can be seen in Fig. 4-5.

The main disadvantage of this control strategy is that besides the generator control is independent of the inverter control, the fact of controlling a constant DC-link voltage with a boost converter will require a non constant current from the generator

since the instantaneous injected power to the grid is not constant (because of the single-phase grid connection). This current variation in the generator side will cause torque fluctuations in the generator, modifying the speed of the turbine. These speed variations can also cause a premature damage to the generator due to the torque ripple produced. With this strategy Maximum Power Point Tracking (hereinafter MPPT) methods can be implemented by controlling directly the injected current with the inverter, but as the injected current is not constant MPPT algorithms are quite difficult to implement and its performance can be somewhat controversial.

A better control strategy for the system can be implemented by using the boost converter to control the power required by the generator and injecting this power with the inverter. In this case, MPPT method will be implemented by varying the requested generator current with the boost converter. The inverter will control in this case the DC-link voltage by injecting power to the grid. With this strategy a constant power in the generator can be achieved and still injecting a non-constant power into the grid. To decouple this power variation from the input and the output side, DC capacitors will act as a power buffer.

With this strategy boost controller will only control the current through the inductor while the inverter controllers will control the DC-link voltage and the injected current.

In Fig. 4-6 it can be seen the block diagram of the boost controller. In this case the current command i_B^* will be calculated by the MPPT algorithm. The MPPT method will be explained in a further section of this chapter. PI regulator will be tuned in same manner than the one presented for the previous control strategy. This is a PI controller with a bandwidth of 500Hz and tuned by cancellation method. The mathematical expression of this regulator can be found in (4.4).

$$k_p = 2 \cdot \pi \cdot bw \cdot L = 2 \cdot \pi \cdot 500 \cdot 5 \cdot 10^{-3} = 15.7080 \tag{4.2}$$

$$k_i = \frac{R}{L} = \frac{1}{5 \cdot 10^{-3}} = 200 \tag{4.3}$$

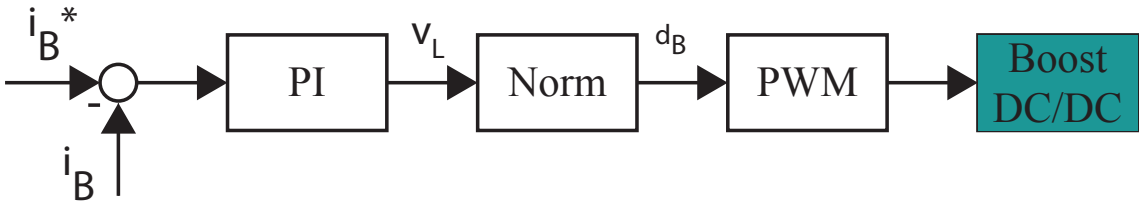

Figure 4-6: Base blocks diagram for boost converter control.

$$\frac{v_L(s)}{i_B(s)} = 15.7080 \cdot \frac{s+200}{s} \left[\frac{V}{A}\right] \tag{4.4}$$

The normalization of the control signal v_L into a duty value can be obtained from (4.5). The demonstration of this equation can be found in the previous project [1].

$$d = \frac{v_l + v_{bus} - v_G}{v_{bus}} \tag{4.5}$$

Block diagrams of the inverter control can be seen in Fig. 4-7. This control is composed of two cascaded control loops: the external one is for DC-link voltage and the inner control loop is for injected current.

The outer control loop is the one in charge of the DC bus voltage. As it was previously said as the input power is constant and the output power cannot be constant due to the single phase connection, bus capacitors will sustain these power fluctuations. As the output frequency is constant, the instantaneous injected power variation will also be fixed to the double of the grid frequency. This means that an oscillation will appear in the bus voltage being double of the grid frequency. To avoid the controller reacting against this voltage variation (it must be remarked that this variation is the normal behavior of the system and it is not a disturbance), a notch filter of that frequency will be included. This notch filter will allow to have a faster regulator that can react to disturbances which frequency is higher than the one mentioned, being insensitive to natural voltage ripple.

The output of the regulator will be the current that is needed to discharge the capacitors to the reference value. If this current is negative it means that v_{bus} is lower than the reference and needs to be charged. If a negative current is requested from

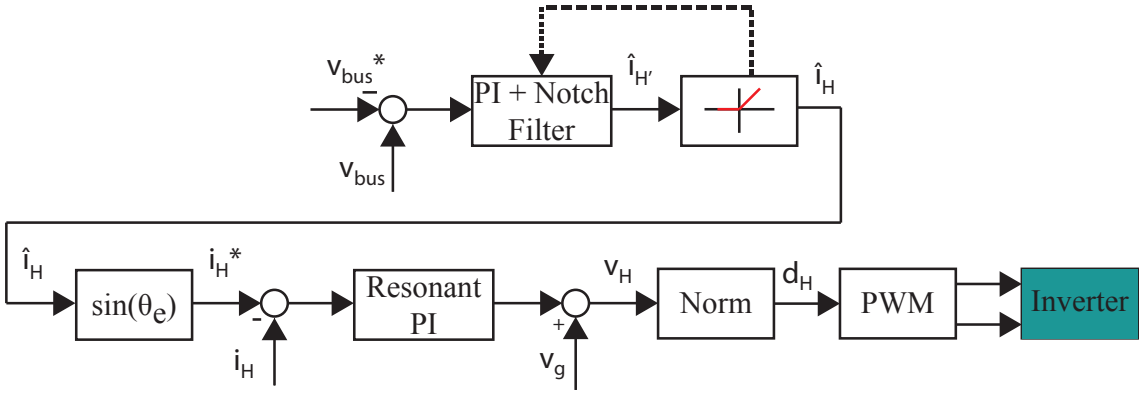

Figure 4-7: Blocks diagram for iverter converter control.

the grid, DC bus capacitor will be charged through the grid becoming the system in a load instead of a generator. To avoid this behavior, the current through the inverter will be limited only to positive values (generation mode). To avoid windup in the regulator this current limit will be complemented with a realizable references algorithm to deal with saturation. This algorithm is based on modify the error to adjust it to the maximum control signal that the system is able to apply.

This voltage regulator will be tuned for a bandwidth of 50 Hz and an overshoot of 5% as it was defined in the previous work. The notch filter included will be at a frequency of 100 Hz and will be -20 dB deep. The expression of the regulator can be seen in equation (4.6) and the Bode diagram for the controller and the notch filter can be seen in Fig. 4-8.

$$\frac{i_H(s)}{v_{bus}(s)} = 0.3690 \cdot \frac{(s+168)\cdot(s^2+14.6\cdots+3.95\cdot10^5)}{s\cdot(s^2+146\cdot s+3.95\cdot10^5)} \left[\frac{A}{V}\right] \tag{4.6}$$

The current reference from the voltage regulator will be the rms value of the current to be injected and must to be converted into the instantaneous sinusoidal value in such a way the power factor of current injected will be one. This is done by multiplying the magnitude by the sine of the phase angle θ_e obtained with the synchronization method explained before. Once the instantaneous current has been calculated a resonant controller will be responsible of inject this current into the grid with no error. This regulator will be the same that the one calculated in the previous project [1]. The final expression for this regulator can be seen in (4.7).

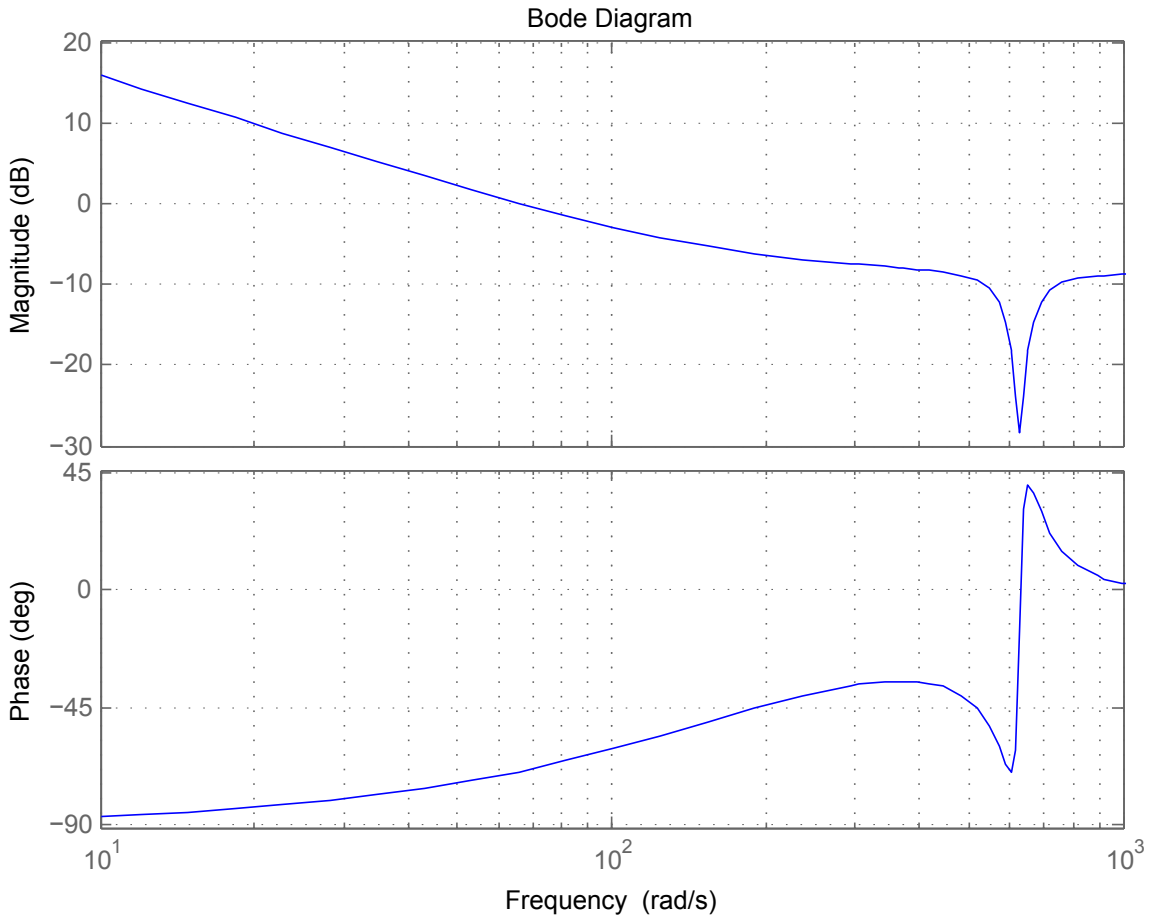

Figure 4-8: Bode diagram for the DC bus voltage regulator with notch filter included.

$$\frac{v_H(s)}{i_H(s)} = \frac{31.42 \cdot s^2 + 6535 \cdot s + 3.101 \cdot 10^6}{s^2 + 9.87 \cdot 10^4} \cdot [\frac{V}{A}] \tag{4.7}$$

As can be seen in Fig. 4-7, the grid voltage will be taken into account as a feed-forward term in order to improve the behavior of the regulator at start-up, improving in this way its dynamics.

4.3 Maximum Power Point Tracking (MPPT) algorithm

The MPPT method is a very important issue in a wind turbine. The chosen method will be determinant relative to wind turbine efficiency. Power of the wind follows a cubic relation with wind speed and also depends on the parameters of the wind turbine, as can be the swept area A or the power coefficient of the wind turbine C_p. As it was explained in chapter 3, this power coefficient is not a constant value, it depends on the tip speed ratio λ and the pitch angle β. A good MPPT method tries to match the λ which gives the maximum performance each time.

As can be seen in [17] there are different methods to get the maximum power from the wind. One of them needs some external data as can be the rotational speed of the turbine or the wind speed, with the inherent increase in cost. Others try to get the correct λ value by slightly modifying actual conditions and looking what happens to the injected power.

To store wind turbine data in a look-up table can be a solution to track the power. In order to use this solution it is needed to have a good knowledge of the power characteristics of the turbine. It is also needed to know either the rotational speed of the turbine or the wind speed [14].

Other methods consist of measuring the actual power that is being extracted by from the wind turbine and modify the current absorbed from the generator. If power increases, more current is demanded, if power decreases, less current is required. This is known as a perturb and observe (P&O) method. The main characteristic of this

method is that a constant power point is never reached, this is continuously oscillating around the maximum power point. This method is implemented in [15].

Alternatively, one interesting method that can be found in [13] is a mixture of both systems. At the beginning the method tries to characterize the wind turbine by implementing a P&O MPPT method. Once it is considered the wind turbine have been correctly characterized, the algorithm changes and behaves as a look-up table which only requires to know the generated voltage.

The method implemented for the present system is not properly a MPPT algorithm, but an approximation of the MPPT curve by a quadratic function. This solution can be done without large errors for low wind speeds where the approximation is very close to the cubic function of the MPPT trajectory. This approximation is not accurate for very low wind speeds, when the turbine is not able to produce energy, and it is also bad for high wind speeds, were the correct values of λ in order to track the maximum power corresponds to values out of range from the ones supported by the turbine. The main idea is to adjust this function in such a way that fits as maximum as possible with the cubic MPPT curve in the working range that for this application is among 5 m/s and 15 m/s. The following demonstration explains the adopted algorithm.

As was indicated in chapter 3, the power that is possible to obtain from the wind turbine can be expressed as (4.8).

$$P = \frac{1}{2}\rho C_p(\lambda, \beta) A v^3 \tag{4.8}$$

where ρ is the air density, A is the swept area and C_p is the power coefficient that is a non linear function of λ (3.6) since the pitch angle β is fixed in this application. λ is the relationship of the rotational speed of the wind and the wind speed as can be seen in (4.9)

$$\lambda = \frac{\omega_r r}{v} \tag{4.9}$$

From (4.8) and (4.9) can be concluded that

$$P_{max} \propto v^3 \propto \omega_{r_{opt}}^3 \tag{4.10}$$

where $\omega_{r_{opt}}$ is the optimum rotational speed which gives a tip speed ratio for a maximum C_p.

As the generator is a Permanent Magnet Synchronous Generator (PMSG), the back electromotive force E is a linear function of the rotational speed [2] (4.11) and the terminal voltage can be obtained from (4.12).

$$E = K_e \Phi \omega_r \tag{4.11}$$

where K_e is a constant and Φ is the generator flux.

$$V_{ac} = E - I_{ac}(R_s + j\omega_e L_s) \tag{4.12}$$

As the generator is connected to the system though a three phase diode rectifier the rectified voltage can be expressed as [3]:

$$V_{dc} = \frac{3\sqrt{3}}{\pi} \cdot V_{ac} \tag{4.13}$$

From (4.11), (4.12) y (4.13) it can be said:

$$V_{dc} \propto \omega_r \tag{4.14}$$

Expression (4.14) can be applied to the system when it is in the maximum power point:

$$V_{dc_{opt}} \propto \omega_{r_{opt}} \tag{4.15}$$

From (4.10) and (4.15) it is possible to say:

$$P_{max} \propto V_{dc}^3 \tag{4.16}$$

This maximum power in the generator can be translated to the DC side in the

system where:

$$P_{dc} = \eta P_{max} = V_{dc_{opt}} I_{dc_{opt}} \tag{4.17}$$

where η is the conversion efficiency into DC. From (4.16) and (4.17), at maximum power point:

$$I_{dc_{opt}} \propto V_{dc_{opt}}^2 \tag{4.18}$$

From (4.18) the maximum power point can be achieved by following a quadratic expression. The approximation that was taken into account for the MPPT was cacculated as the linearization of (4.18) in the working range of the turbine (5 m/s - 15 m/s). From the power curves obtained in chapter 3 and applying expressions 4.11 and 4.17 current-voltage curves of the turbine can be obtained. This curves are shown in Fig. 4-9 where the maximum power points are marked with '+'. The linearization of the MPPT path is in purple.

The trajectory for the MPPT approximation was calculated as the straight line that passes through maximum power points for a wind speed of 5 m/s and for 15 m/s. In Fig. 4-10 it is shown the power that is possible to obtain for a wind speed and the power that is able to track with the proposed method. The error between both trajectories is small compared with the one that can be produced by measurement errors due to the uncertainty of the sensors, being the largest deviation of 1.66% produced for a wind speed of 13 m/s where it is obtained 1482 W instead of 1507 W.

4.4 Over-current and over-speed protections

One of the disadvantages of the variable speed micro wind turbines is that they have to be exposed to a large variations of current and speed. It must be noted that when speed changes, according to expressions (4.11) and (4.12) voltage also changes. Current limitations are determined by the thermal behavior and the resistance of the components, voltage limitations are determined by the rating of the components.

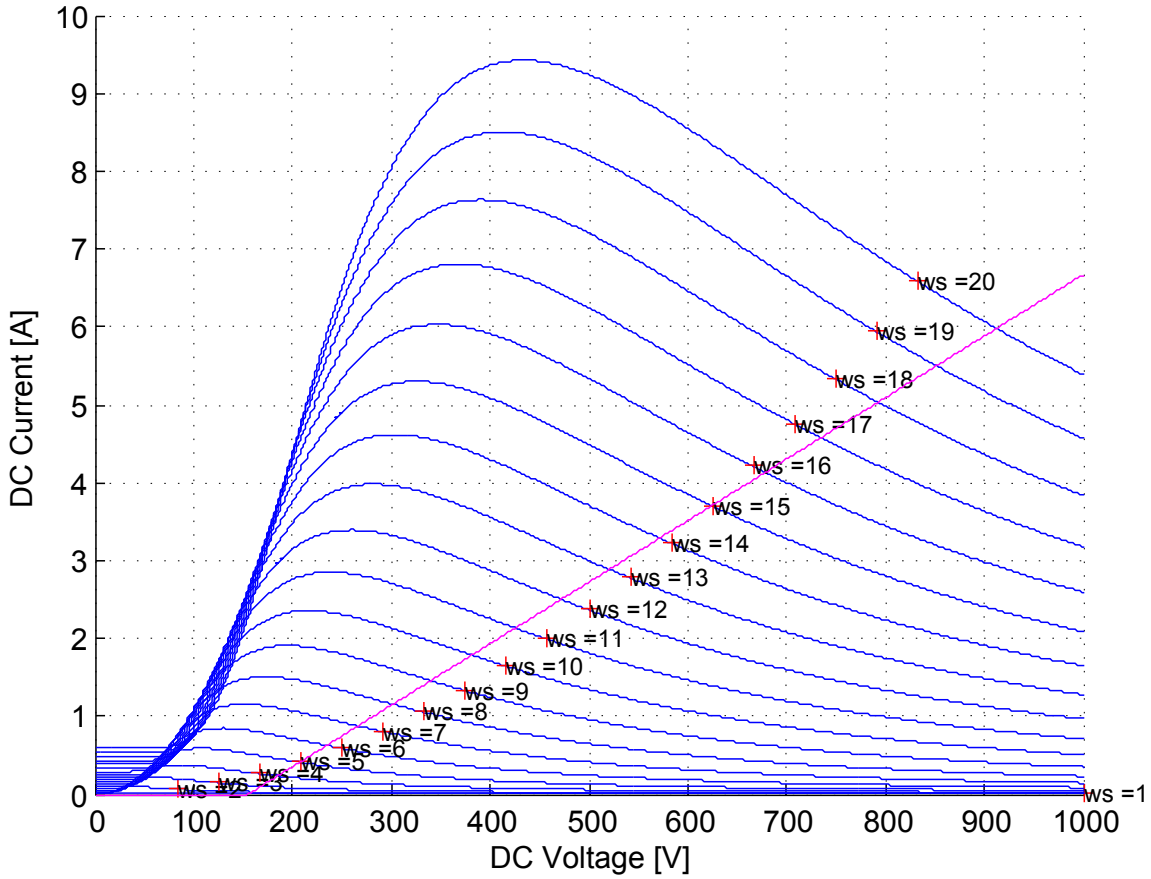

Figure 4-9: Current-voltage characteristics of the wind turbine.

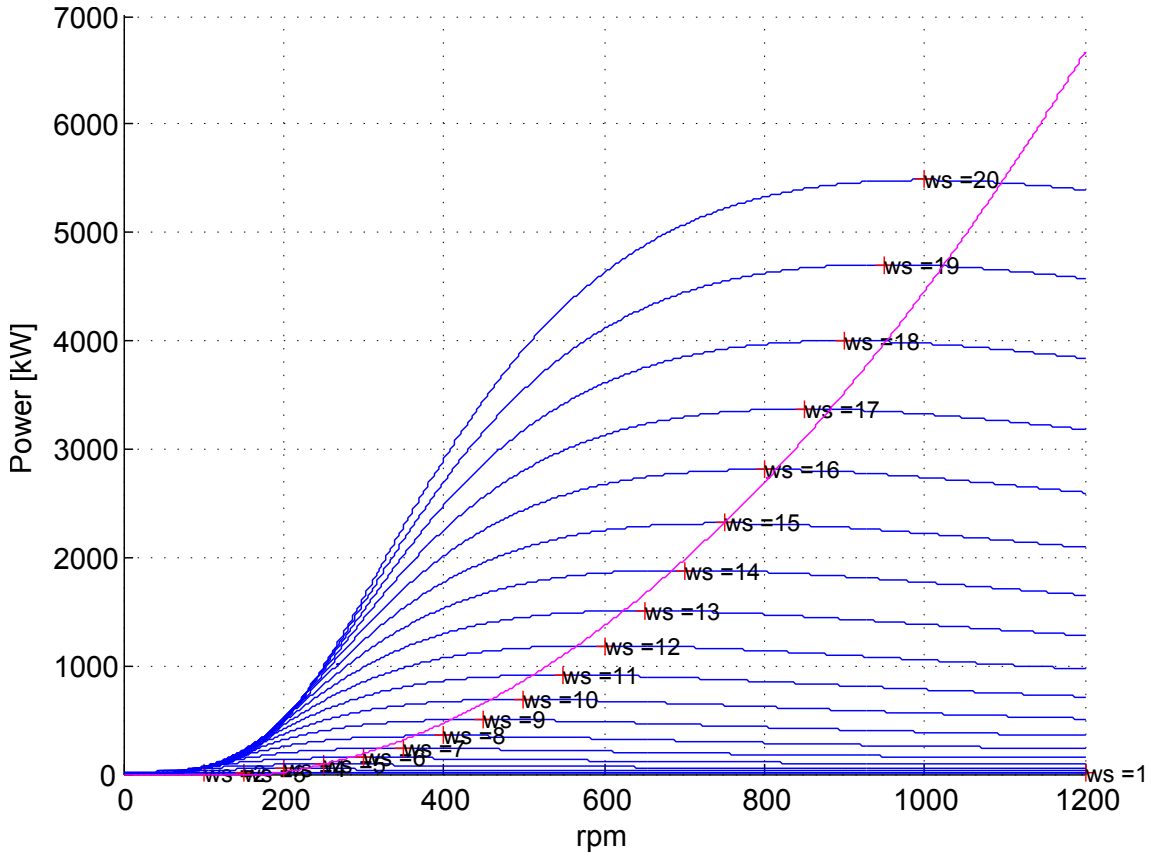

Figure 4-10: MPPT approximation trajectory compared to real power curves.

Typically, a component is more suitable to withstand over-voltages than over-currents. Once it is reached the voltage limit of a component this component is immediately damaged forever meanwhile an over current can be sustained a certain period of time before the component is permanently damaged.

For this kind of systems an over-voltage condition can be easily reached during the whole life of the system due to high wind speeds. Looking at Fig. 4-9 it can be noticed that when the wind blows too strong, the maximum power point is at one speed that can not be achieved by the system. One simple solution for this problem is to stop the wind turbine at the cost of losing energy.

A solution for this issue is to keep injecting power even when the wind speed is high by keeping the turbine at a fixed speed. This solution requires to move away from the maximum power point at high wind speed in benefit of keeping the turbine generating.

It is interesting to put in practice this protection without the need of changing the control structure, avoiding sudden jumps in voltage or current references and keeping the turbine under control in every moment. With these protections included in the turbine control, the transition among the limits will be done in a natural way, being these changes very smooth.

The method presented in this Master Thesis is a new new control strategy presented here first time.

4.4.1 Over-speed protection

A high speed can produce an over-voltage that can cause damages in the electronic components of the system. This is why it is important to keep the turbine working in an acceptable speed range apart from the vibrations that can be produced in mechanical components of the turbine.

The idea of this protection is to allow the system to track the MPPT algorithm when the speed of the turbine is in the design range and try to brake the turbine when it is out of limits, moving away from the MPPT trajectory. The goal of this protection is to keep the turbine at the maximum speed when this limit is reached,

preventing to the turbine to speed-up when the wind is too strong.

This protection can be done by applying more electric torque in the generator when it is needed to reduce speed. As the torque is proportional to the active current demanded from the motor, this protection can be implemented requesting more current when it is needed to reduce the speed.

In order to be able to control the current requested from the motor, it is important to have enough control signal (ie. current) to do this. This means that v_{bus} have to be higher than the voltage of the generator v_{dc}, so the limit for the generator voltage have to be lower than the DC bus voltage reference, leaving some margin for the ripple produced because of the single-phase power injection. A reasonable margin value is 100 V for this particular system. This margin can be increased by using better voltage sensors with less noise. It can be also increased including in the controller an anti-windup algorithm.

Looking at the current-voltage curves (Fig. 4-9) of the wind turbine, in order to decrease the voltage generated by the turbine and therefore its speed, it is needed to increase the amount of current requested from the generator, in order to keep constant the speed. In Figure 4-11 it can be seen the trajectory that must to be followed in order to track the maximum power point with over-voltage protection. Notice that the MPPT algorithm has been modified reducing the linearized points, linearizing it between the minimum power point 5 m/s and the maximum power point closer to the voltage limit, in this case 12 m/s.

In order to avoid changes in the control architecture that can cause undesired transients in the behavior of the system, a voltage regulator will be included to the base control scheme seen in Fig. 4-6. This controller will control the rectified voltage of the generator by modifying the requested voltage. One of the problems including this regulator is that when the voltage is lower than the maximum voltage, the regulator could request negative current in order to try to speed-up the generator. This cannot be done due to the diode rectifier and also is not the desired operation mode because if the voltage is lower than the voltage limit, MPPT algorithm must be followed. In order to avoid negative references in the requested current, this regulator

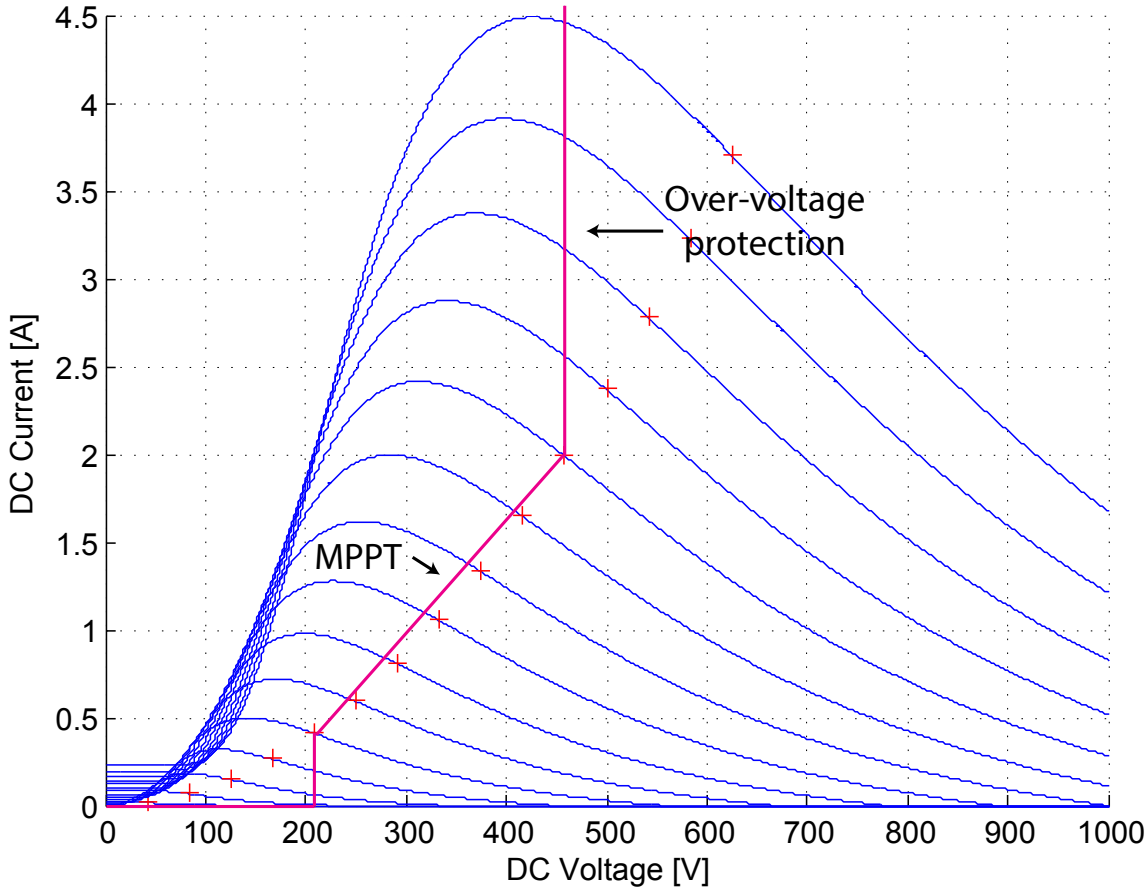

Figure 4-11: Trajectory of the MPPT approximation with over-speed protection.

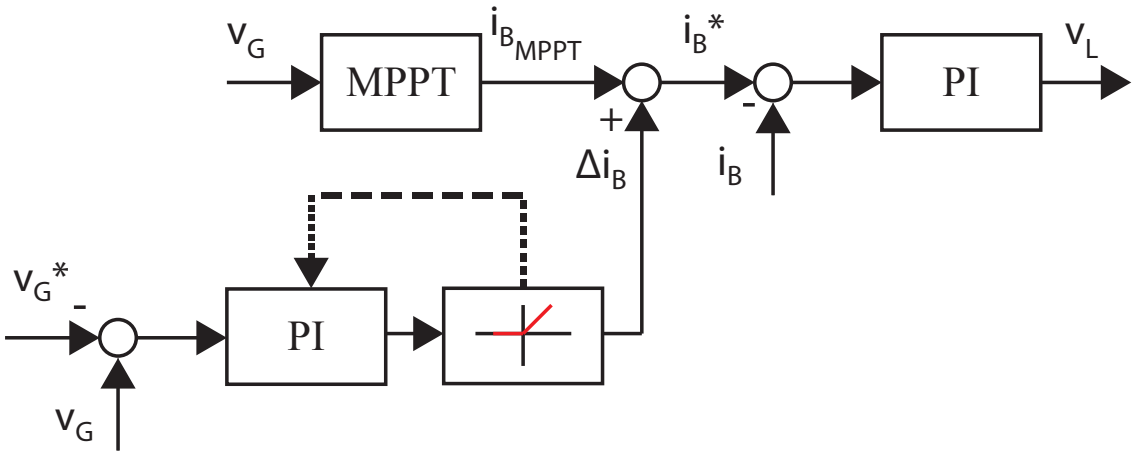

Figure 4-12: Boost control blocks diagram for MPPT and over-speed protection.

will be limited to only positive values. In order to avoid windup, realizable references will be implemented.

The output of this regulator will be added to the current demanded from the MPPT algorithm, in this way, when the voltage is lower than the maximum one, the current demanded will be only the one requested by MPPT being the current requested by voltage regulator zero. Once reached the voltage limit, MPPT will require the correspondent amount of current and the voltage regulator will require the correspondent current to provide the needed torque and keep the speed in range. The block diagrams for this controller can be seen in Fig. 4-12.

The PI regulator will be tuned to control the generator speed taking into account its inertia. The bandwidth for this regulator (4.19) is 10 Hz and will be tuned for a maximum overshoot of 5%:

$$\frac{\Delta i_B(s)}{v_G(s) - V_{G_{max}}} = 0.3690 \cdot \frac{s + 168}{s} \left[\frac{A}{V}\right] \tag{4.19}$$

4.4.2 Over-current protection

The over-voltage protection has been explained in the previous subsection, but it is not enough to protect the system against high power values. Until now if the wind is too strong, the speed of the turbine is kept to a maximum value. If this maximum limit is kept constant, the power generated will also increase with the wind speed, increasing

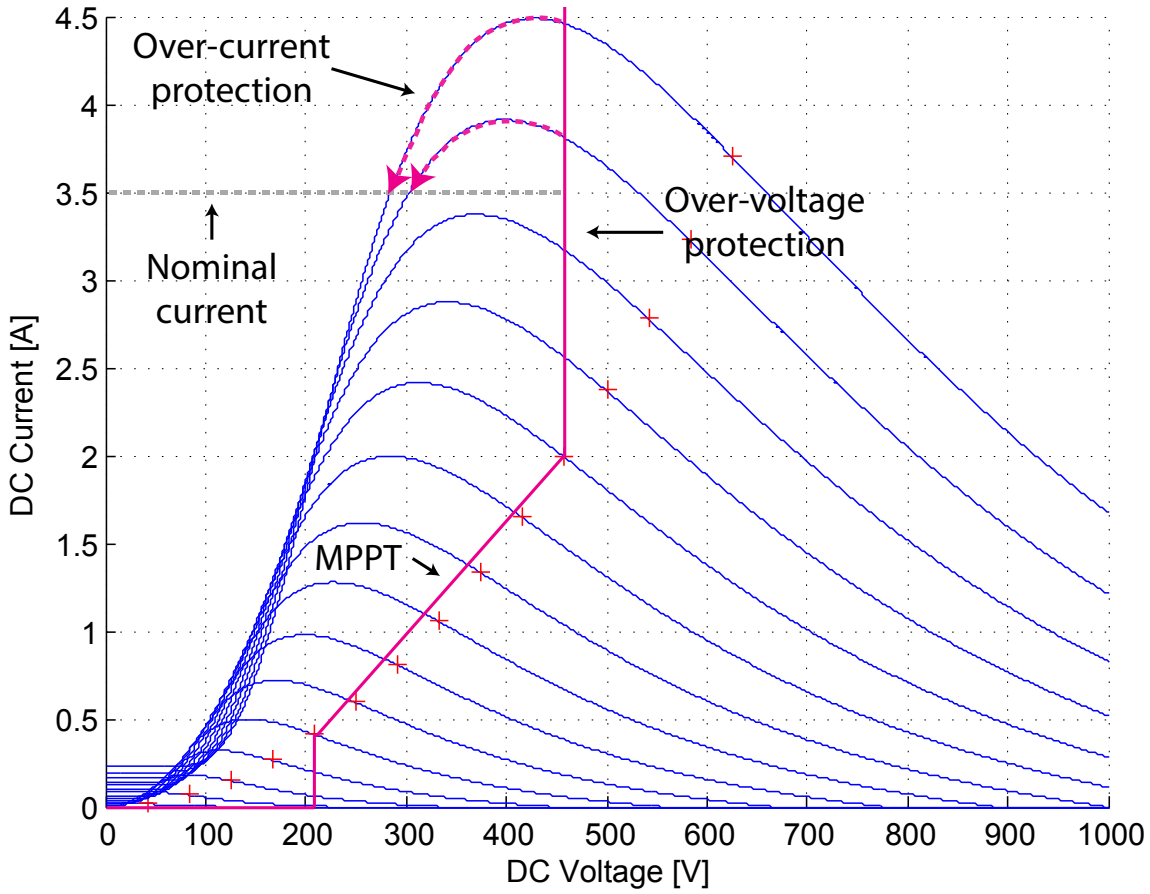

Figure 4-13: Trajectory of the MPPT approximation with over-speed and over-current protections.

also the current that flows through the converter. This high currents can damage the converter so it is also important to protect the system against over-current.

The increase in current can produce over-heating of components and some of them can eventually fail. This is the reason why it is also important to keep the current among limits. As it was mentioned before, components can often handle more current than the rated one for a short period of time, but after this time, they get damaged due to overheating. Looking at the power curves, there is a region where the power decreases for all wind speeds when the speed decreases. The proposed method try to move the operation point to this region where voltage an power can be controlled without surpassing the limits of the system.

This protection must also allow the system to track the maximum power point when the wind conditions are among limits, and also be compatible with over-voltage

protection. The idea is that once the rated current of the system is over passed, the voltage is reduced (therefore the speed of the turbine) in such a way that the current needed to maintain the turbine in that voltage fits with the nominal current of the system. This trajectory can be seen in Fig. 4-13. While moving through the curves, current can be higher than the nominal one, this is the reason why the nominal value must not fit with the maximum peak current that is possible to handle.

The maximum value of the current in the system must be higher than the peak that can be produced when the turbine is is speeding-down. Due to the shape of the current curves, there will be a maximum of the current to be handled in the interval between 0 and the maximum voltage limit whatever the wind speed be. If the peak current is higher than the one supported by the system, voltage limit must be decreased to fit the maximum current value of the turbine among that range with the peak value of the components.

In order to implement this protection in such a way that the system behaves naturally without sudden changes, this protection will be made decreasing the voltage limit when the current is higher than the nominal one. This will be done integrating the current difference between the nominal one and rated. In order to avoid a voltage limit increase, this regulator will be limited only to negative values, and in order to not completely stop the turbine the voltage reference cannot be lower than 250 V in order to allow to the turbine to generate. To avoid windup issues realizable references will be used. In Fig. 4-14 can be seen the blocks diagram for both, speed and current protections.

4.5 Simulation of the system

A simulation of the system was performed with the aim of testing the behavior of the system, implementing the control strategy explained in this chapter. Although each control loop was tested separately, here it will be only presented the simulation of the complete system, trying to follow a full wind profile.

The profile chosen for the wind simulation, must contain several speed variations

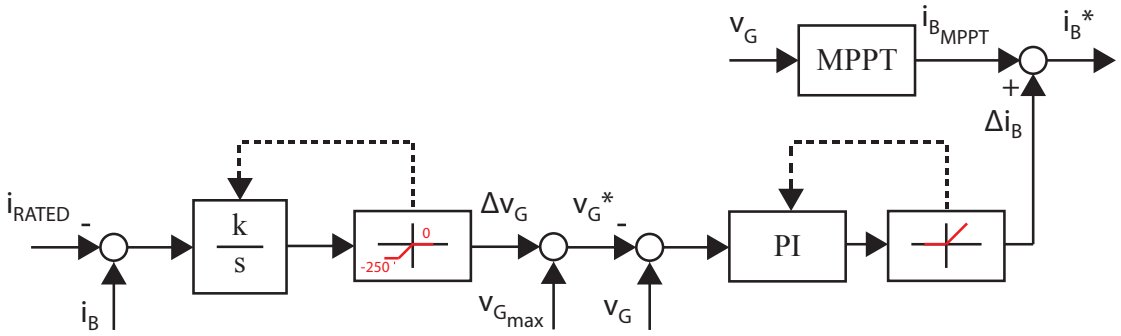

Figure 4-14: Boost control blocks diagram for MPPT with over-speed and over-current protection.

in order to test the system under very different conditions, trying to get a simulation as much complete as possible. All the components will be parametrized in consonance with the real components to be used, this means that all parasitic components as can be ESR in capacitors and inductors will be taken into account as well as the R_{ON} and voltage drop of the semiconductors. To simulate the behavior of the wind turbine, a wind turbine model following the expressions presented in Chapter 2 will be used.

In Fig. 4-15, it can be seen in the upper part the wind speed profile used for the simulation and in the lower part the maximum instantaneous power that the turbine can deliver. This profile have regions where the power is smaller than the nominal power and the turbine can follow the MPPT trajectory. Winds over 13 m/s can cause over-voltages in the turbine so the system must keep the voltage controlled once this limit is surpassed.

Fig. 4-16 shows the current and voltages resultant from the simulation. It can be seen how the bus voltage is constant along the whole simulation (except during start-up). This voltage has a 100 Hz ripple since the power injected into the grid is not constant while the power taken from the generator is constant at steady-state. This can be seen in Fig. 4-17 where it is presented a detail of these results.

In Fig. 4-16 it can be seen how the current increases with the input voltage, following the relationship explained in previous sections. Once the voltage reaches 450V (the voltage limit for this case), current continues increasing in order to maintain the turbine speed controlled.

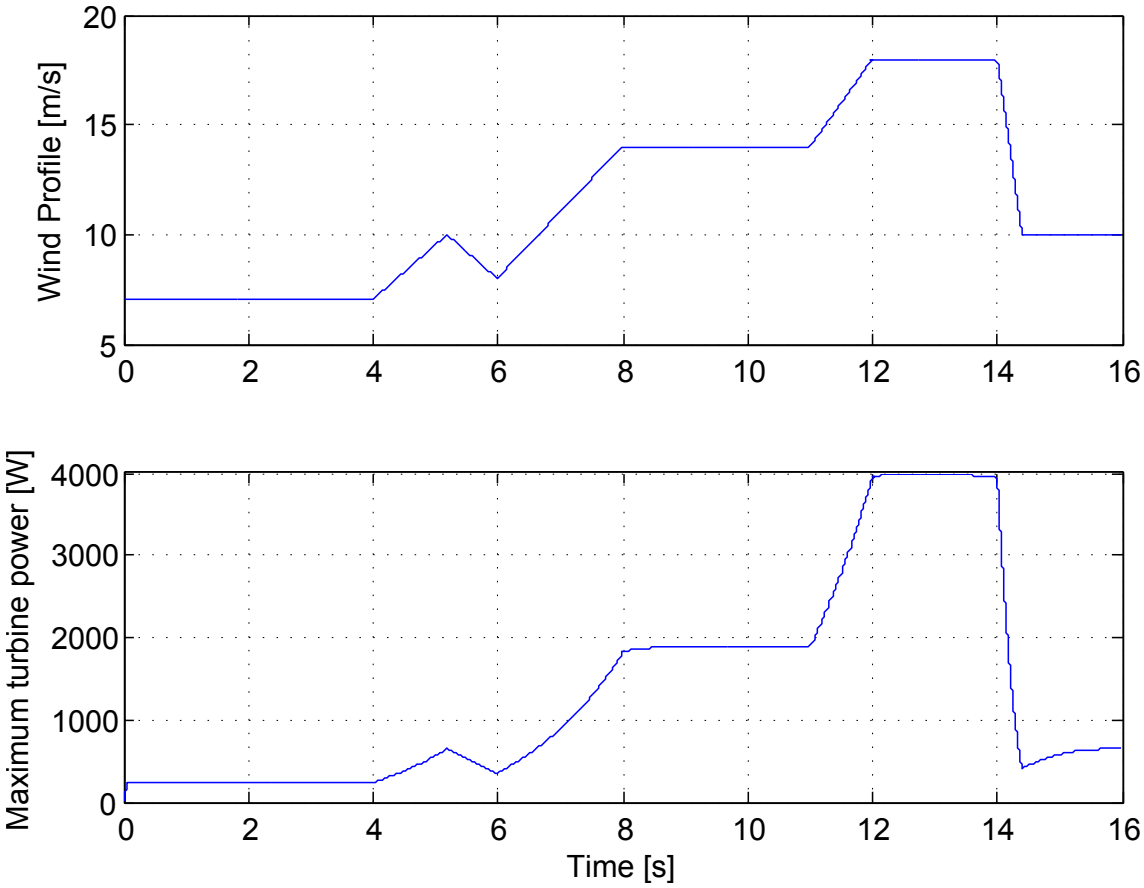

Figure 4-15: Wind speed and power profile used for simulation purposes.

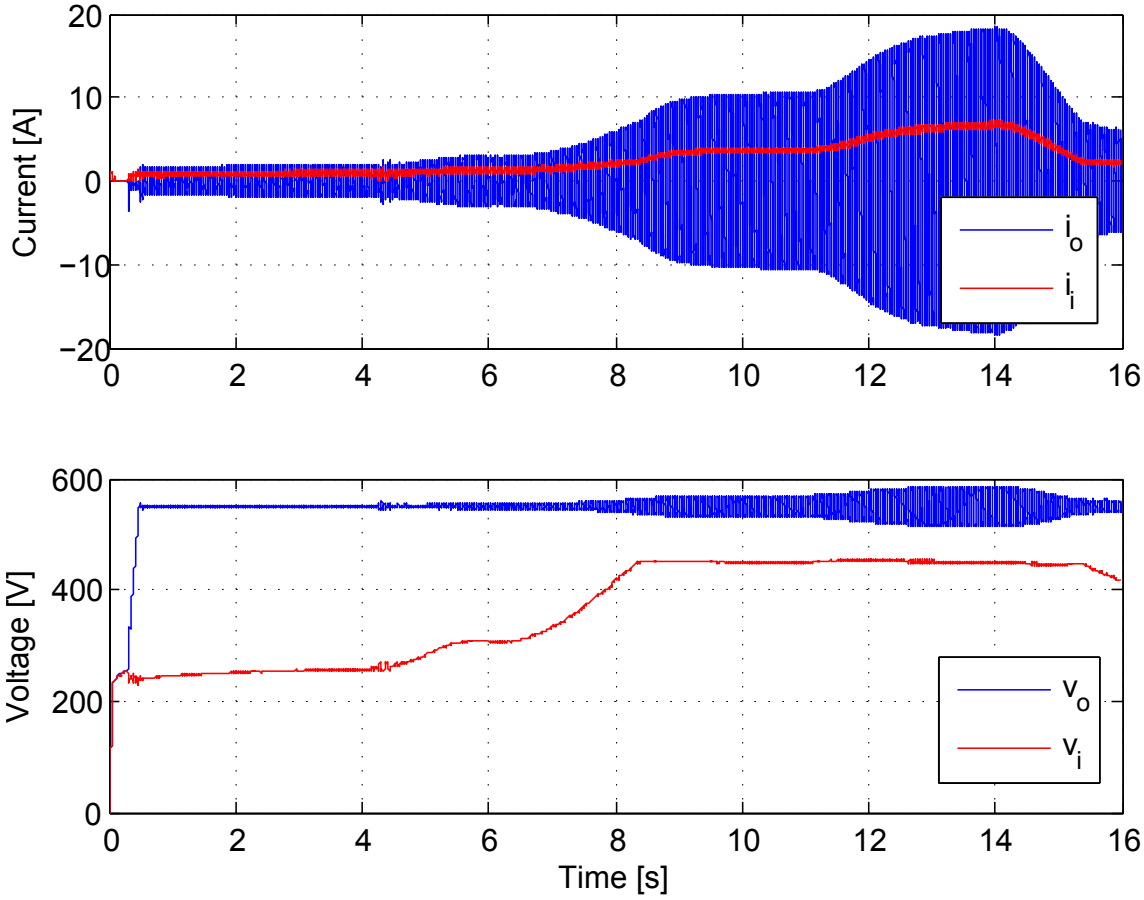

Figure 4-16: Current and voltage (simulation results).

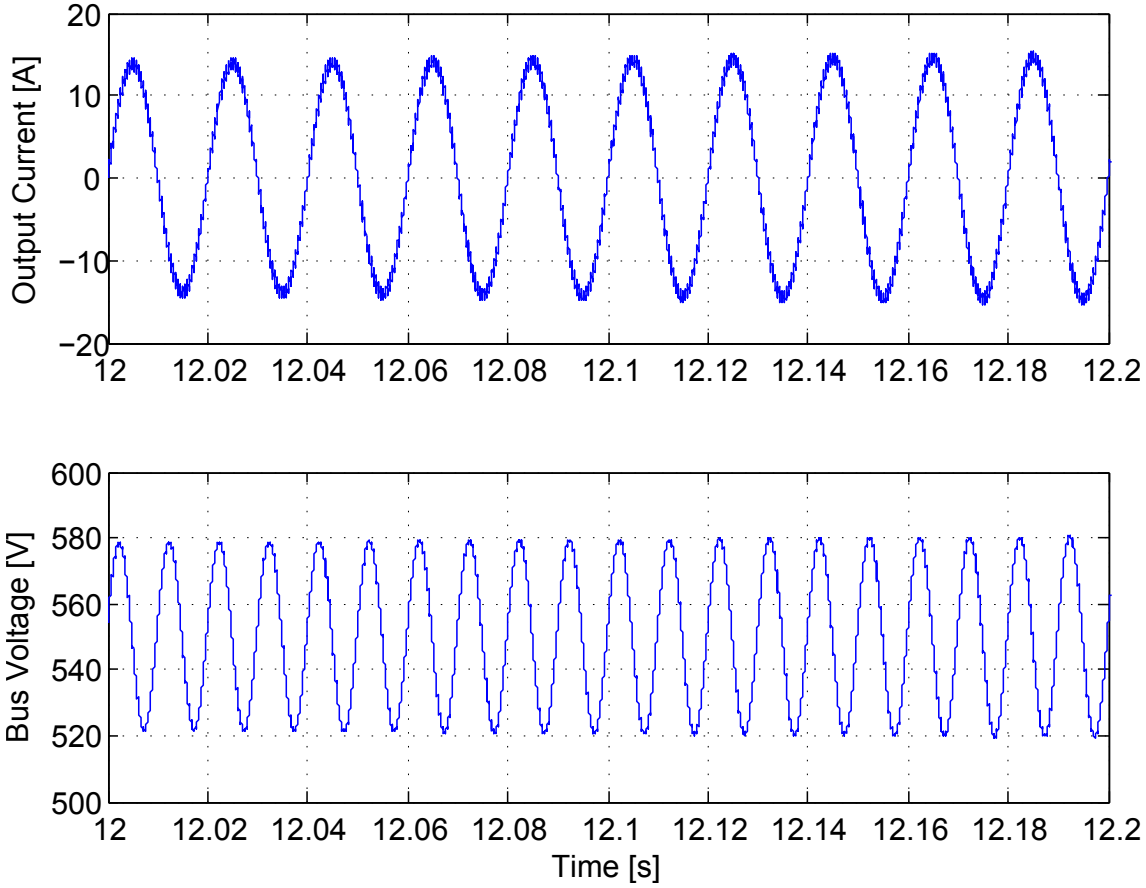

Figure 4-17: Detail of output current and voltage waveforms for a wind speed of 18 m/s (simulation results).

The output current also increases when the input current does. This occurs because the bus voltage must to be kept constant, so it is needed to inject more current in order to avoid charging the capacitors. The ripple amplitude of the bus voltage is dependent on the output current level but the frequency is fixed to 100 Hz.

4.6 Experimental results

Simulation results have been presented in previous section, where different wind speed changes have occured. In order to compare this simulation results the same wind profile will be applied to the actual system. This profile will be programmed in the frequency converter as a time dependent function.

In order to start-up the motor, this wind profile will not start from a zero wind speed, but from 7 m/s.

In this test, all control loops and protections have been implemented, not as in the simulation case where over-current protection was not implemented due to model limitations. In this case the applied wind profile is the same. The results for this test can be seen in Fig. 4-18 where it is presented the injected current measured in the line, the rectified generator voltage measured at the output of the rectifier, and the DC bus voltage measured in the bus capacitors. In can be seen how the response is similar to the simulated one taking into account that in actual test the inertia comes only from the generator plus the induction motor coupling. Input current cannot be presented due to there is no room to place the current probe in the PCB. Notice that in order to start-up the motor, this wind profile will not start from a zero wind speed, it will start from 7 m/s.

In this experimental case, voltage protection is working for winds speeds higher than 14 m/s. It can be seen how the system keeps the voltage to the maximum value. Over-current protection occurs when the wind speed is 18 m/s. A high current is being demanded from the turbine, so the system reduces the input voltage trying to find a point in the power curve where both voltage and currents are in range. Once the wind speed is below these limits, the system continue following MPPT trajectory.

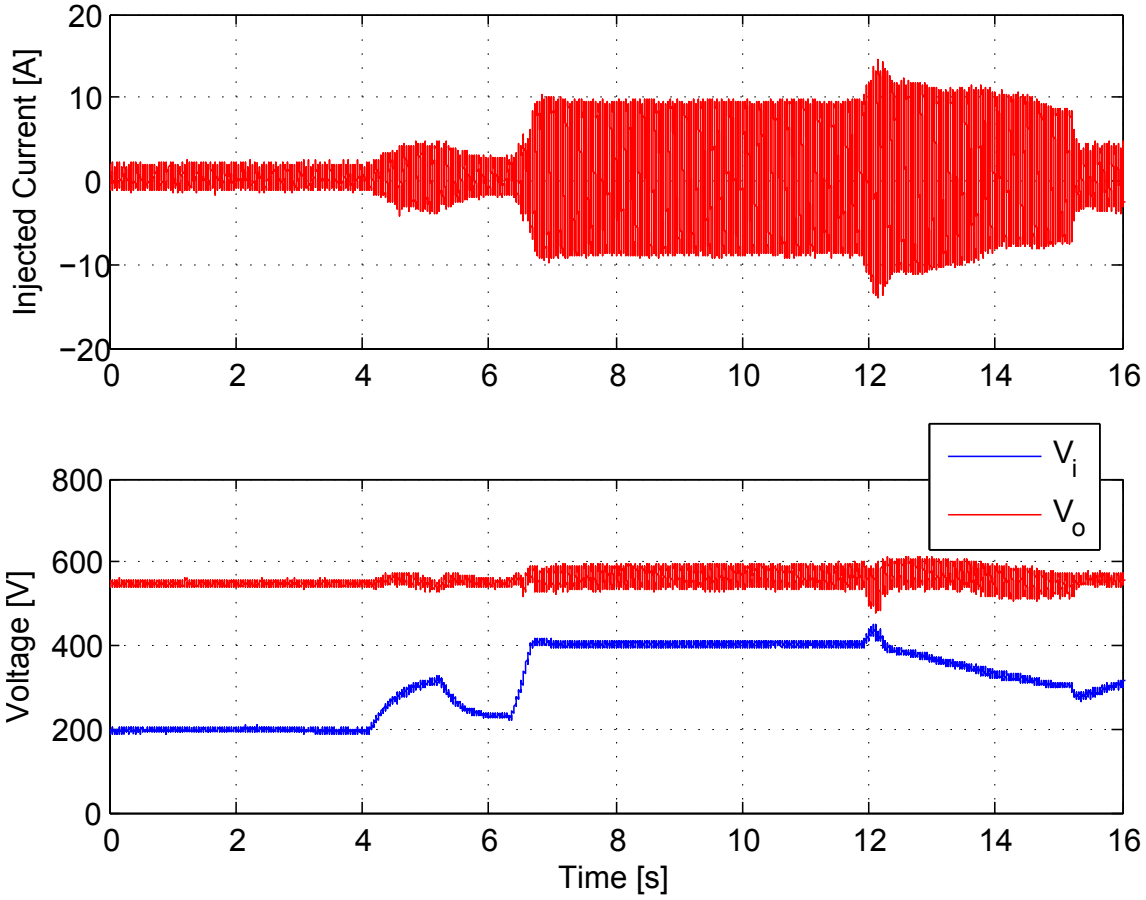

Figure 4-18: Current and voltage (experimental tests).

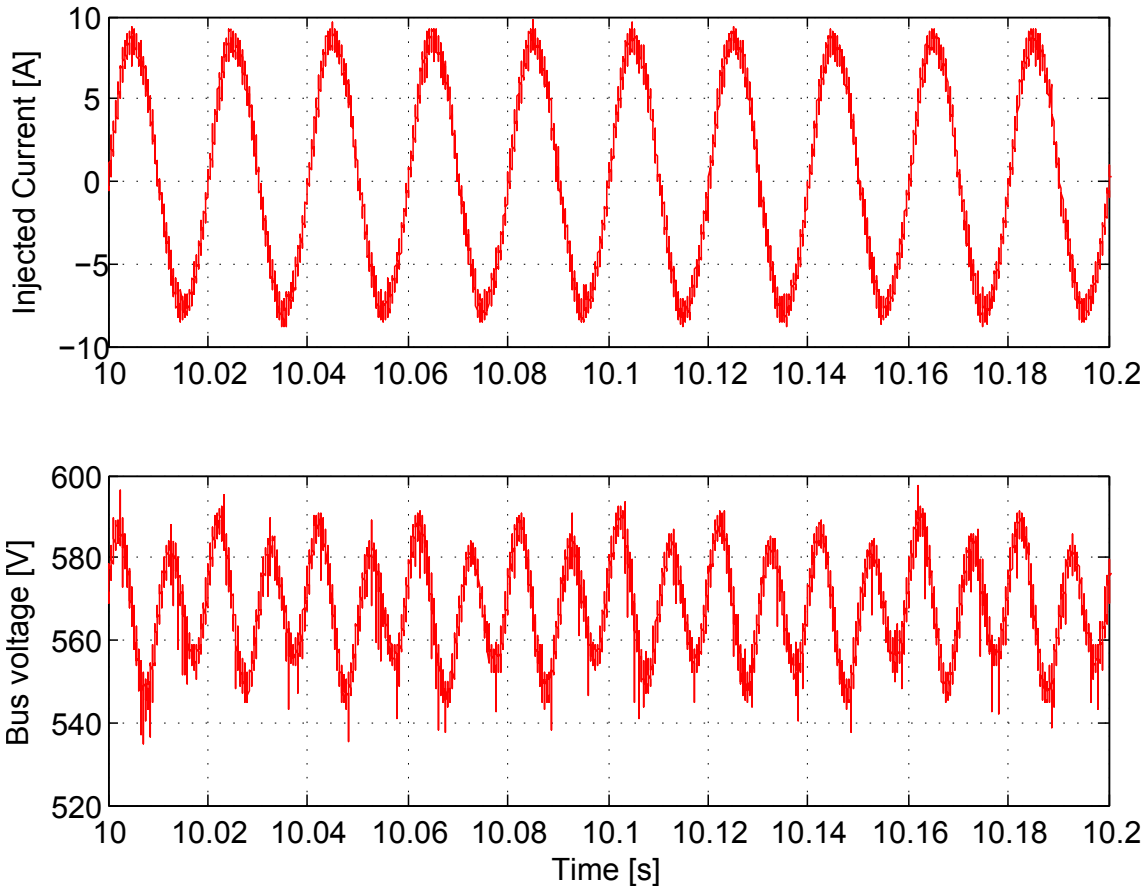

Figure 4-19: Detail of output current and voltage curves for a wind speed of 14 m/s (experimental tests).

During the interval between 5 and 6 s, it can be seen how the voltage decreases more than in the simulation case, this is because in the experimental test the only inertia that was present was the generator one. This is why the speed of the generator, and hence the voltage, have faster dynamics.

In Fig. 4-19 it can be seen a detail of the injected current and DC bus voltage. In this case there also can be seen the voltage ripple in the bus voltage which frequency is double of the grid frequency.

Chapter 5

Communication system

As it was introduced in the previous project, an interesting part from the point of view of commercialization of a product is providing a communication module that enable the user to monitor some data relative to the generation process. It is also interesting from the point of view of commercialization to provide the user with some tool to control the turbine, this may include the chance of starting/stopping the turbine, or decrease its maximum speed during the night with the aim of decrease the noise, making the system more competitive and appealing.

But this is not only interesting from the point of view of the commercialization, it can be also interesting for debugging processes, where it is needed to check some parameters or measurements avoiding to store data in a memory, allowing to see what is happening in real time.

In the present project, the communications module will be handled only for debugging purposes, but the same design can be also used in a commercial application by modifying the data to be sent.

In order to meet the market trends, a WiFi module will be chosen due to this technology is broadly extended and it is very common to find it in any personal computer. The WiFi module chosen is *WiFly RN-174* from *Roving Networks* company.

This module will create its own network to which is possible to connect with any WiFi device (PC, mobile phone, etc.). Once the socket is established, the generating system will act as a server and will be waiting for a client. This connection can be

done by opening a socket from a client. Once the socket is opened, the communication process can start.

From the point of view of handling this module in a DSP, it can be connected though the SCI or in a future version of the WiFi module it can be through SPI which is faster than SCI. In this case SCI module will be used.

For debugging process, DSP will be continuously sending data to the module, which only will send the data over WiFi if a socket has been opened from a client. The data to be sent are the actual power taken from the turbine, the current that is being taken from the generator and a status variable. This status variable contains useful information from control strategy as could be if the turbine has entered in speed control mode or if some alarm occurred. This variable will also be useful as acknowledgment of the commands sent to the system from the client applications as could be the stop order.

In order to interact with the turbine, an application client was developed. This interface has been written in visual C with *Embarcadero Studio RAD XE3* previously known as *Borland C++ Builder*. This tool allows to create an application with the basic interface elements needed as can be charts to represent data, a log screen, or buttons to give functionality to the system.

This application is ready to show the actual generating values, check if one event has occurred, or send commands to the turbine such as Start/Stop the turbine or decrease its speed. Also, it will have a button to open or close the socket, controlling this way the communication path. A snapshot of this application can be seen in Fig. 5-1.

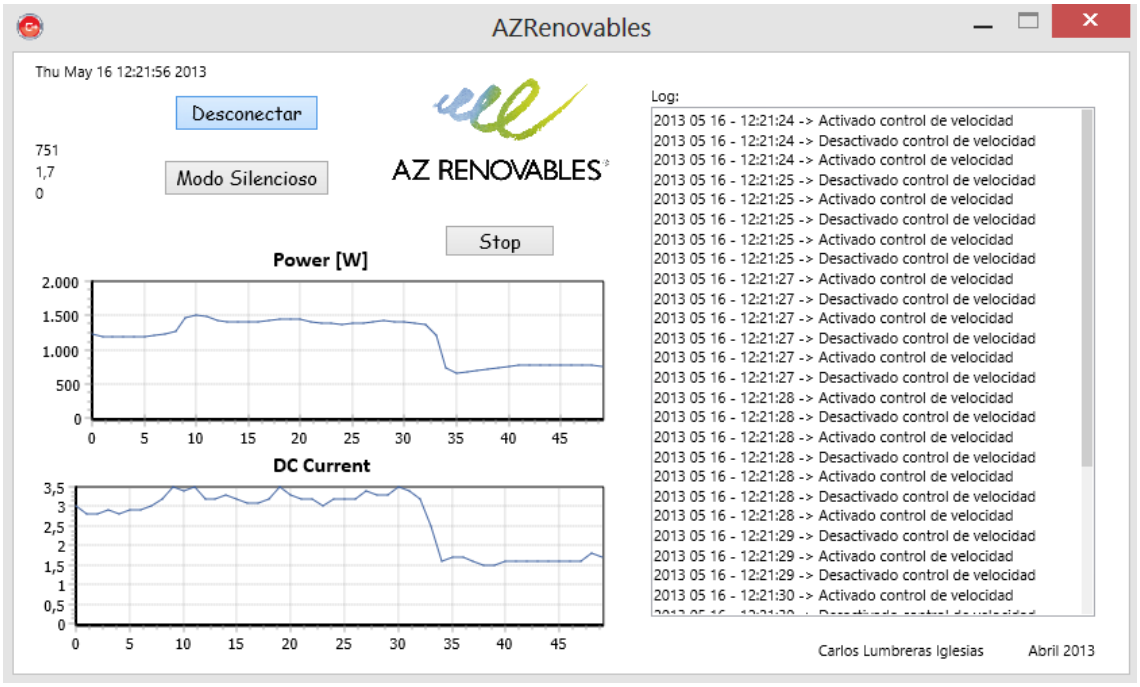

Figure 5-1: Snapshot of the PC application for communications.

Chapter 6

Regulations

Every product intended to be marketed has to comply with all regulations concerning the product. Due to the commercial nature of this system, this chapter is included in order to study the actual regulations. This project only covers to the electrical part of the system, so it only will present the regulations concerning the electrical system, in this case to comply with Spanish regulation.

The regulations that are going to be studied here are the ones related with grid connection conditions, electromagnetic compatibility (EMC) and harmonics. Due to some test require to check the behavior of the system as a whole, some of them cannot be done because the case is needed to pass the test.

6.1 General connections

According to BOE number 295 from December 15th 2011, RD 1699/2011 November 18th by which is regulated the grid-connection of small scale power production facilities. every system intended to be connected to the grid must do it under some specific conditions. The technical conditions needed to connect a system to the grid are presented in this RD and must to be complied with.

In regular working conditions, the system must not cause disturbances the network higher than the admissible ones. In the case that a distribution line is disconnected from the grid, the system must not provide voltage to the grid for safety issues. There

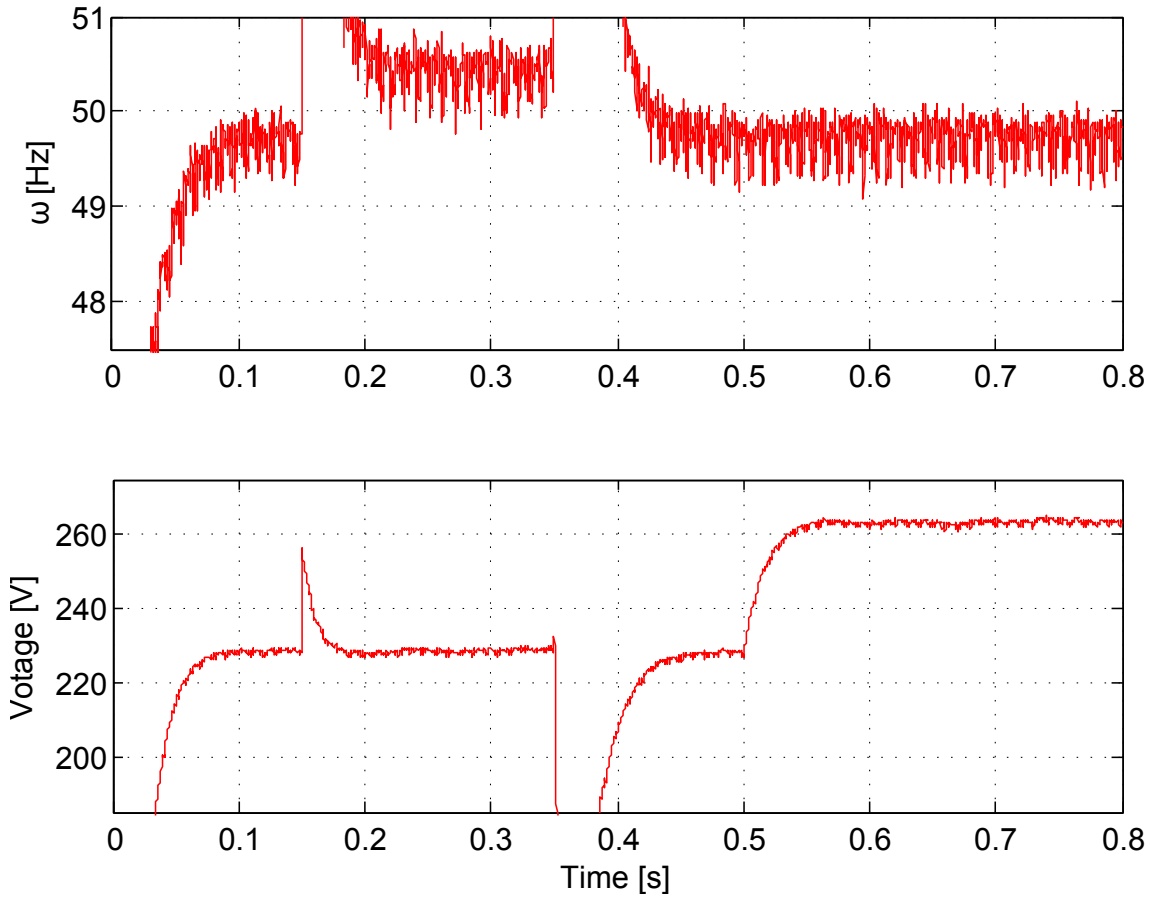

Figure 6-1: Response time of the PLL.

can only be one single connection point by each single installation.

Concerning the power of the system, in the same regulation it is indicated that the maximum power for a single phase system is 5 kW, otherwise the system must be a balanced three-phase system (admissible an unbalance of as much 5 kW). The power factor of the installation must be higher than 0.98 when it is operating over 25% of the rated power.

The system must to be well protected, providing it with all automatic and differential protections as required in article 4 of the mentioned RD. This protection must be done with mechanical devices in order to break the current path and can not be done by using semiconductor devices.

For our particular case, the system has a single-phase connection since its maximum power is 2.5 kW. The power factor of the system is very close to unity factor

Parameter	Threshold	Response time
Over-voltage	u_n +10%	1.5s
Over-voltage	u_n +15%	0.2s
Minimum voltage	u_n -15%	1.5s
Maximum frequency	50.5Hz	0.5s
Minimum frequency	48Hz	3s

Table 6.1: Response time for frequency and voltage level protection required by regulations

for all power ranges, specially when the power is high since the current is controlled every moment.

In order to provide protections, relays has been placed in the system in order to connect or disconnect from the grid, being this relays mechanical and no semiconductor devices.

Concerning to maximum/minimum frequency protections and maximum/minimum voltage protection the system table 6.1 shows the limit values that must to be complied.

In case of maximum frequency fault, the system must stay disconnected until the frequency be less or equal 50 Hz.

With PLL explained in chapter 4, it is possible to detect frequency and voltage changes very fast. In order to test this , a 230 V and 50 Hz signal was perturbed. In time t=0.15 s, the frequency goes from 50 Hz to 50.5 Hz and in time t=0.35 s the frequency returns to 50 Hz. In time t=0.50 s but the voltage increases 15%. In Fig. 6-1 it can be seen the results of this test. It can be noticed as all changes has been noticed by the PLL very fast, allowing the protection to be faster enough to comply with the regulations, detecting the voltage increase in less than 0.1 s while the regulation requires 0.2 s.

Earthing conditions are also required by the regulation, however, according with EN 61000-6-3 and EN 61000-6-4 earthing requirement are compliant if lightning protection regulations are also compliant, which are more restrictive. This lightning protection mus be evaluated as a whole system needing the complete system (case, blades..) in order to test the earthing connection.

According with article 15 point 2 in EN 61000-6-4, the installation must have a galvanic isolation among the distribution network and the generator. This means that it is needed to install a transformer to connect it to the grid. This transformer can also act as a filter behaving both as galvanic isolation and as a filter. This transformer cannot be formed with semiconductors.

Due to the system is a prototype, the transformer has not been placed yet, being the filter the only device between the system and the grid. In a commercial application this transformer must be taken into account.

6.2 Electromagnetic Compatibility (EMC)

All electronic devices must comply with Electromagnetic Compatibility regulations. It exists a specific standard for EMC in wind turbines. This standard is UNE-CLC TR 50373. In this regulation are presented all the issues that must be taken into account for EMC test and refers to the specific regulation that deals with this issue in detail. The regulations to be met with depend on the final placement of the system, being different if the system is going to be installed in industrial or residential environments.

In this case, the system is going to be connected to a low voltage public distribution grid and it will be placed near residential, commercial or light industrial places, so it must comply with EN 61000-6-2 and EN 61000-6-3, which are the strictest standards. In these standards are defined the the limits of emission and immunity to electromagnetic fields.

Immunity is a measure of the ability of electronic products to tolerate the influence of electrical energy (radiated or conducted) from other electronic products and electromagnetic phenomena. The limit and the reference to the corresponding test can be found in EN 61000-6-2.

Emission limits and the reference for the specific tests can be found in EN 61000-6-3.

According to UNE-CLC TR 50373 the CEM test must to be passed with the system fully mounted. This is why no test EMC test were take into practice with the

Harmonic Order	Present [%]
1	100
3	13.78
5	5.05
7	5.59
9	1.57
11	1.05
13	0.75
15	0.57
17	0.44
19	0.35
21	0.29
23	0.24
25	0.20

Table 6.2: Maximum Amplitudes of Harmonic Currents [18]

PCB.

In order to make this test, it could be carried out at the Prodintec facilities at the University of Oviedo, where can be done all the test needed to obtain the CE mark.

If the test are not successful, it can be added to the system an on-board electromagnetic interference (EMI) filter. There are two kind of EMI filters, narrowband EMI in case of exceed emission limits or broadband in the case of surpass immunity limits.

There are commercial EMI filters that can be easily adapted to the system that depends on the voltage level and the attenuation needed. These filters will be included in case they were needed.

6.3 Harmonic distortion

One of the main issues concerning the developed system is the harmonic content of the injected current. This is a low power system and can be connected to a single phase network. However, a large number of inverters tied to the same feeder can cause problems if the inverter's harmonics are excessive. This is why IEEE recommends certain values for the harmonics that is better not surpass. Those values are presented in table 6.2

This is only a recommendation given by IEEE, the mandatory standard for measuring and evaluating the quality of supply characteristics for wind turbines connected to the grid is UNE-EN 61400-21. Here there are included all magnitudes that must be stipulated to characterize the power quality of a wind turbine as can be voltage fluctuations, connection operations, active and reactive power, and current harmonics.

The most relevant issue for this type of systems are the harmonics injected into the grid. As it is included in the standard, these harmonics have to be measured in different portions of the rated power: 0, 10, 20 ... 100% of P_n. Regulation requires specify the harmonic content up to frequencies 50 times higher than the grid frequency.

Inter-harmonic current components must be specified up to 2 kHz according to IEC 61000-4-7:2002, and high frequency components must be evaluated from 2 kHz to 9 kHz. All these harmonic analysis must be evaluated for a unity power factor.

In order to analyze the results of the harmonic content, it is recommended by UNE-EN 61400-21 to use a window length of 10 cycles for a 50 Hz system and 12 cycles for a 60 Hz system. Discrete Fourier Transform (DFT) must be applied with a rectangular ponderation. This window can also be used to calculate active power.

According to UNE-EN 61400-21 and IEC 61000-4-7:2002 the Total Harmonic Current (THC) must be evaluated as follows:

$$THC = \frac{\sqrt{\sum_{h=2}^{50} I_h^2}}{I_n} \tag{6.1}$$

where I_h is the harmonic content for the harmonic subgroup h and I_n is the fundamental harmonic.

For harmonic components lower than 2 kHz, must be split into groups according to IEC 61000-4-7:2002 annex A:

$$C_{isg,n}^2 = \sum_{i=2}^{8} C_{k+i}^2 \tag{6.2}$$

For harmonic components from 2 kHz to 9 kHz they have to be measured and grouped according to annex B in IEC 61000-4-7:2002. The output of the DFT must

be grouped in 200 Hz bands.

$$Gb = \sqrt{\sum_{f=b-90(Hz)}^{b+100} C_f^2} \tag{6.3}$$

In order to correctly evaluate the harmonics content, it is needed to take samples of 10 minutes length. With the actual equipment, it is not possible to store 10 minutes with an adequate sampling rate. In order to evaluate the system the length of the samples was reduced to 1 minute in order to evaluate the system. In order to evaluate IEC 61000-4-7:2002 a digital power analyzer (e.g. DPA 500N from emtest) will be needed.

In Fig. 6-2 it can be seen a portion of the window used to analyze the harmonic content for the current corresponding with $\frac{2}{3}$ of the rated power. In the top of this figure, it can be seen the grid voltage measured, in the middle the current measured and in the bottom, for the sake of better understanding can be seen the generator voltage and the bus voltage.

In Fig. 6-3 it can be seen the spectral analysis of the current seen in Fig. 6-2 corresponding to a wind speed of 12 m/s. The THD will be calculated in base to this data according to (6.1) and (6.2). The THD for this current up to 2 kHz is 0.0264 and for frequencies from 2kHz to 9 kHz, according to (6.1) and (6.3) is $0.52077 \cdot 10^3$.

According to UNE-EN 61000-3-2, this system is a Class A type because the maximum current is less than 16 A and does not fit in classes B, C or D. In this regulation are present the limits for the harmonics of the injected current. These admissible values are shown in table 6.3

The harmonic content for a wind speed of 12 m/s can be seen in table 6.4. It can be seen how all values are between ranges complying with UNE-EN 61000-3-2.

The worst case in therms of harmonics is when the value of the injected current is too low and the power of the harmonics can be higher than the power injected with the fundamental harmonic. The case presented in Fig. 6-4 corresponds to a wind speed of 7 m/s and the power injected is 128 W which is less than 10% required to comply with harmonic regulations.

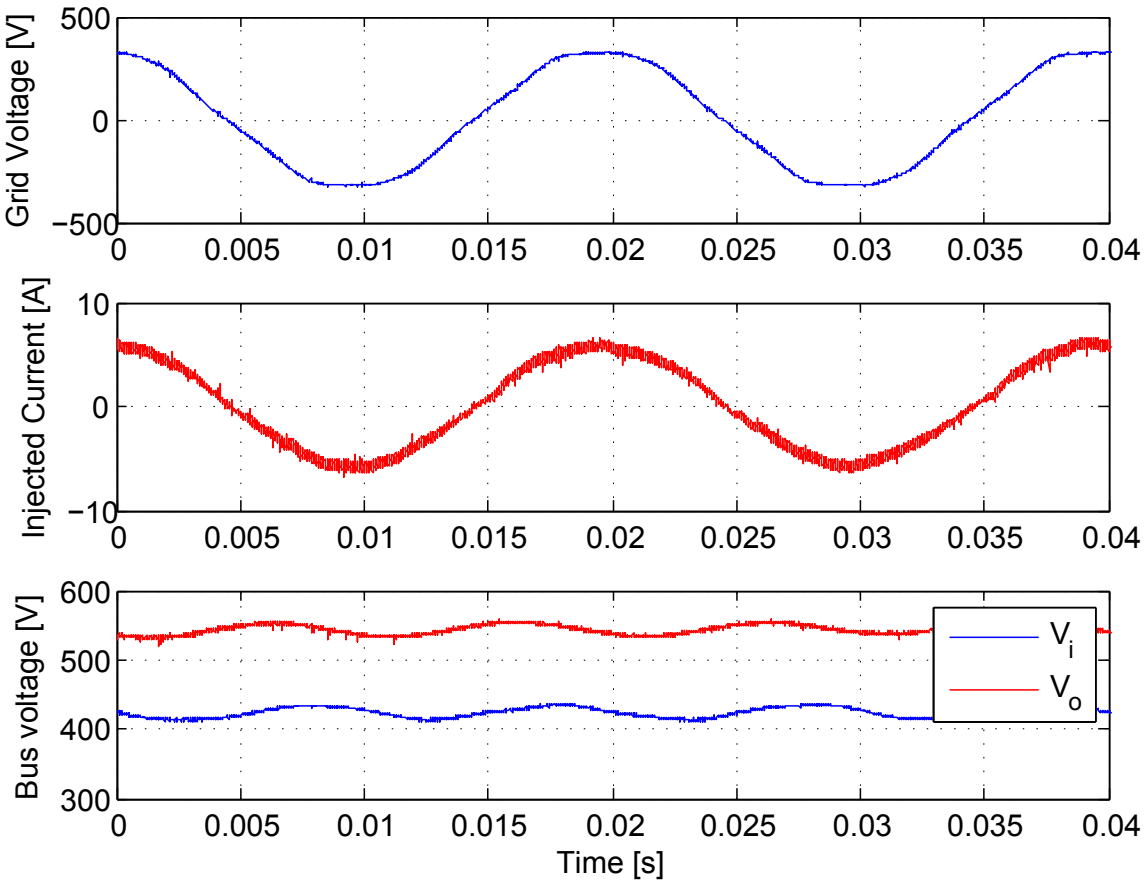

Figure 6-2: Real generation data corresponding to a wind speed of 12m/s.

Harmonic Order	Maximum harmonic current [A]
Odd harmonics	
3	2.30
5	1.14
7	0.77
9	0.40
11	0.33
13	0.21
$15 \leq n \leq 39$	$0.15\frac{15}{n}$
Even harmonics	
2	1.08
4	0.43
6	0.30
$8 \leq n \leq 40$	$0.23\frac{8}{n}$

Table 6.3: Maximum Amplitudes of Harmonic Currents admissible by UNE-EN 61000-3-2.

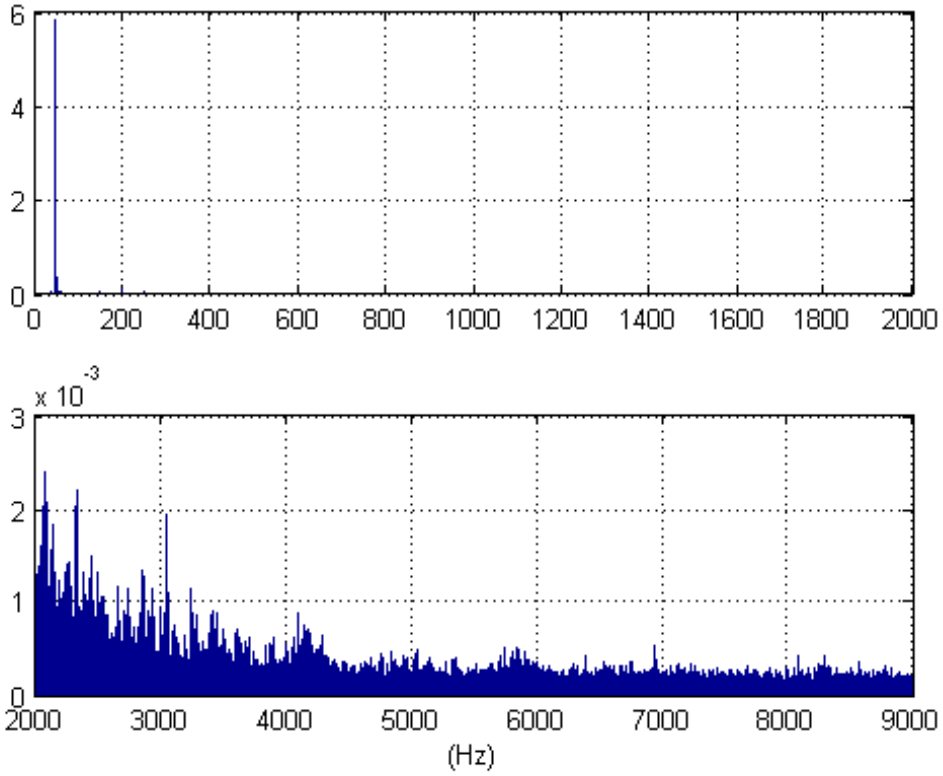

Figure 6-3: Frequency spectrum for the current injected for a wind speed of 12m/s.

Harmonic Order	Maximum harmonic current [A]	Measured current [A]
Odd harmonics		
3	2.30	0.080
5	1.14	0.054
7	0.77	0.028
9	0.40	0.021
11	0.33	0.008
13	0.21	0.000
15	0.12	0.004
17	0.11	0.001
19	0.10	0.003
21	0.09	0.003
23	0.08	0.003
25	0.07	0.002
27	0.07	0.001
29	0.06	0.001
31	0.06	0.001
33	0.06	0.001
35	0.05	0.001
37	0.05	0.001
39	0.05	0.000
Even harmonics		
2	1.08	0.026
4	0.43	0.100
6	0.30	0.047
8	0.23	0.005
10	0.18	0.008
12	0.15	0.005
14	0.13	0.002
16	0.12	0.007
18	0.10	0.002
20	0.09	0.002
22	0.08	0.000
24	0.08	0.001
26	0.07	0.002
28	0.07	0.002
30	0.06	0.001
32	0.06	0.001
34	0.05	0.001
36	0.05	0.001
38	0.05	0.001
40	0.05	0.000

Table 6.4: Harmonic content for 7m/s.

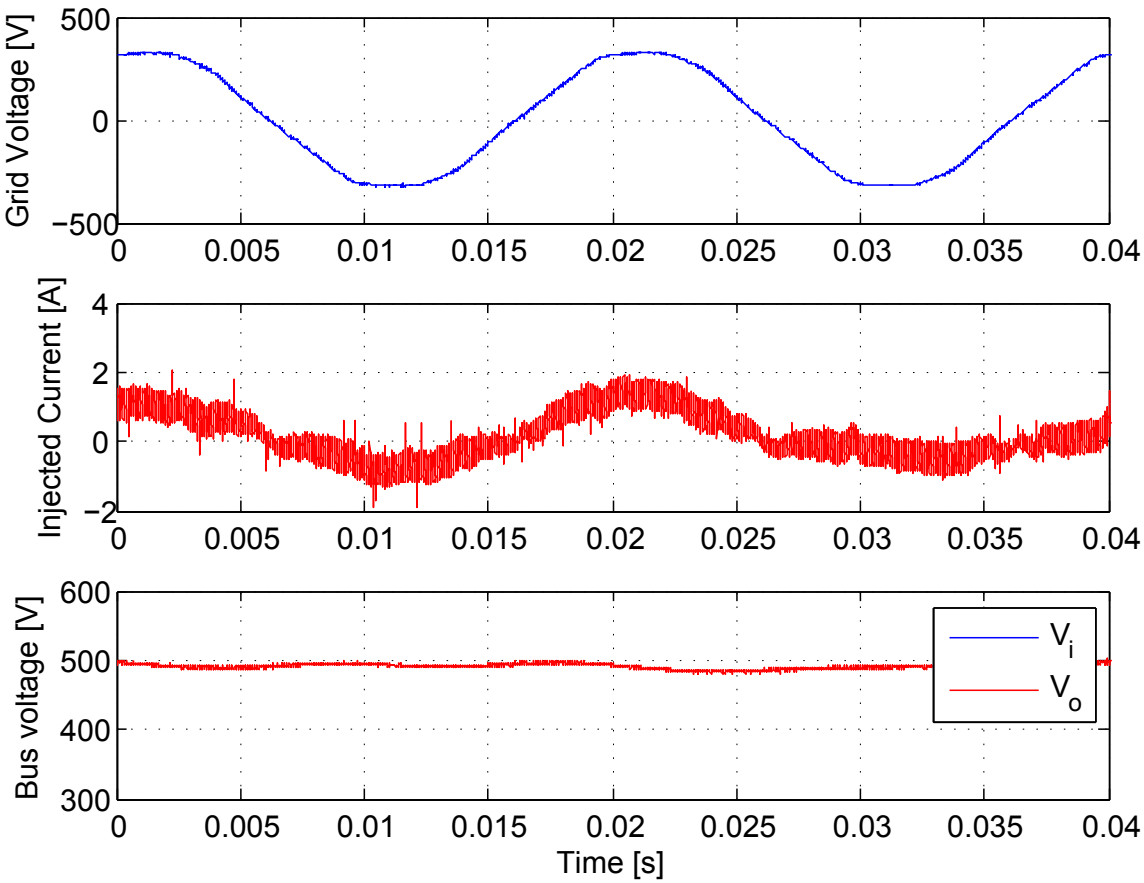

Figure 6-4: Real generation data corresponding to a wind speed of 7m/s.

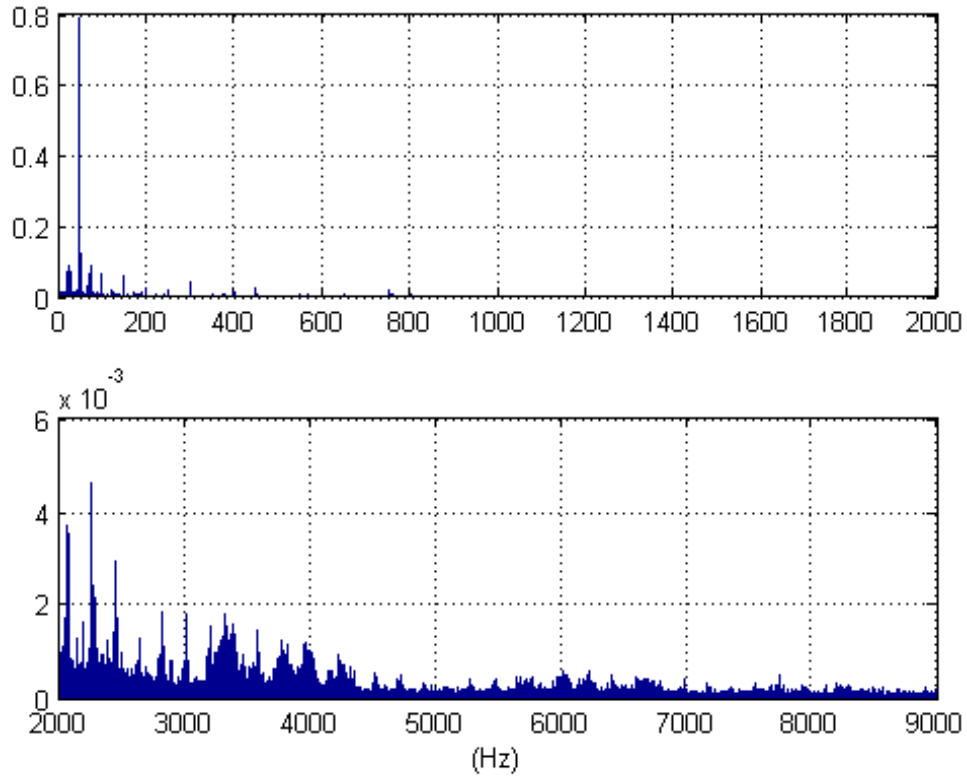

Figure 6-5: Frequency spectrum for the current injected for a wind speed of 7m/s.

In Fig. 6-5 it can be seen the spectral analysis of the current seen in Fig. 6-4 corresponding to the current for a wind speed of 12 m/s. The THD will be calculated in base to this data according to (6.1) and (6.2). The THD for this current up to 2 kHz is 0.1173 and for frequencies from 2kHz to 9 kHz, according to (6.1) and (6.3) is 0.0039.

The harmonic content for a wind speed of 7 m/s can be seen in table 6.4. It can be seen how all values are between ranges complying with UNE-EN 61000-3-2.

Harmonic Order	Maximum harmonic current [A]	Measured current [A]
Odd harmonics		
3	2.30	0.060
5	1.14	0.008
7	0.77	0.000
9	0.40	0.006
11	0.33	0.001
13	0.21	0.002
15	0.12	0.003
17	0.11	0.002
19	0.10	0.005
21	0.09	0.001
23	0.08	0.001
25	0.07	0.001
27	0.07	0.001
29	0.06	0.001
31	0.06	0.001
33	0.06	0.001
35	0.05	0.001
37	0.05	0.001
39	0.05	0.000
Even harmonics		
2	1.08	0.066
4	0.43	0.019
6	0.30	0.004
8	0.23	0.005
10	0.18	0.001
12	0.15	0.001
14	0.13	0.000
16	0.12	0.001
18	0.10	0.001
20	0.09	0.000
22	0.08	0.001
24	0.08	0.001
26	0.07	0.001
28	0.07	0.002
30	0.06	0.001
32	0.06	0.001
34	0.05	0.001
36	0.05	0.001
38	0.05	0.001
40	0.05	0.000

Table 6.5: Harmonic content for 7m/s.

Chapter 7

Conclusions and future developments

In this Master Thesis it has been presented a generation system for a small wind turbine. This work is based in a previous design which needed to be improved in therms of control and hardware. The goal of this Master Thesis is to improve the system solving some difficulties that was found during its design.

Here was presented some changes to make the system autonomous and more reliable, introducing some changes in the hardware design as can be the current sensors or the power sources. Here was demonstrated that all changes done were successful and the system is able to work standalone. The PCB shape was also changed being now prepared to integrate the system inside the nacelle of the wind turbine.

Also here was presented a new control strategy that allows the system to work near the maximum power point of the wind turbine, improving the global efficiency of the system. Although the algorithms implemented are not though to fit the maximum power point, they are very close to this maximum and the power difference between them can be considered negligible (near 1%). These algorithms was implemented without the need of adding more sensors than the needed for controlling the system. Wind speed and rotational speed are not measured to track the maximum power point.

Apart of a valid control that able the system operate with the maximum efficiency, here was introduced new methods to protect the system from high speeds and powers that could damage the system, allowing the system work under very hard wind conditions safely. These protections are presented here first time and can be object of improvement in a further work.

Along the development of this Master Thesis all the new control concepts introduced were tested by simulations and its validity was confirmed by experimental results. This confirms that the system is suitable for wind power generation.

7.1 Future developments

As a future work, is pending to pass the test needed to comply with all the regulations and standards introduced in this Master Thesis.

Here was presented some new concepts that need to be deeply studied in order to improve its behavior. Over-current protection can be a good starting point. Until now, when it is need to reduce the power injection of the system, the speed was decreased to a non fixed point. This point depends on the actual wind speed. One way to improve its behavior is to study how the system can be carried to a determined point where the system is safe for all wind speed without lessen the efficiency of the system more than needed.

Appendix A

Experimental setup. Graphical description

In this appendix you can find some photos of the system.

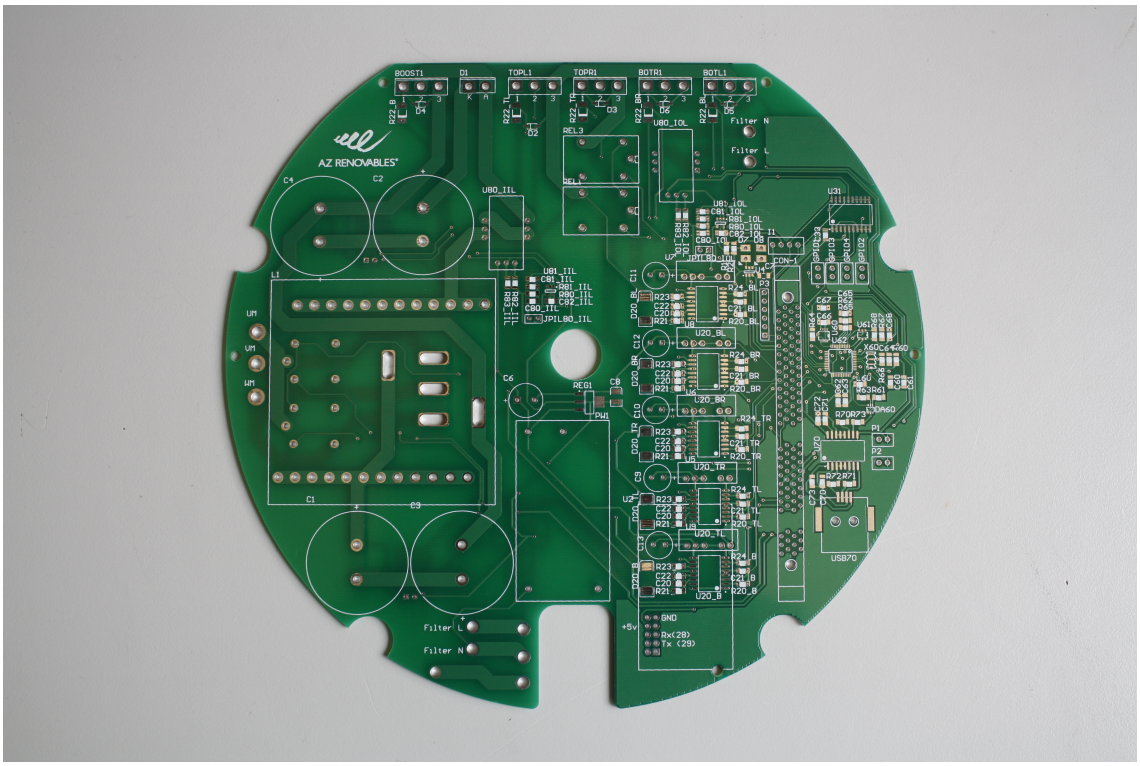

Figure A-1: Top Layer of the PCB

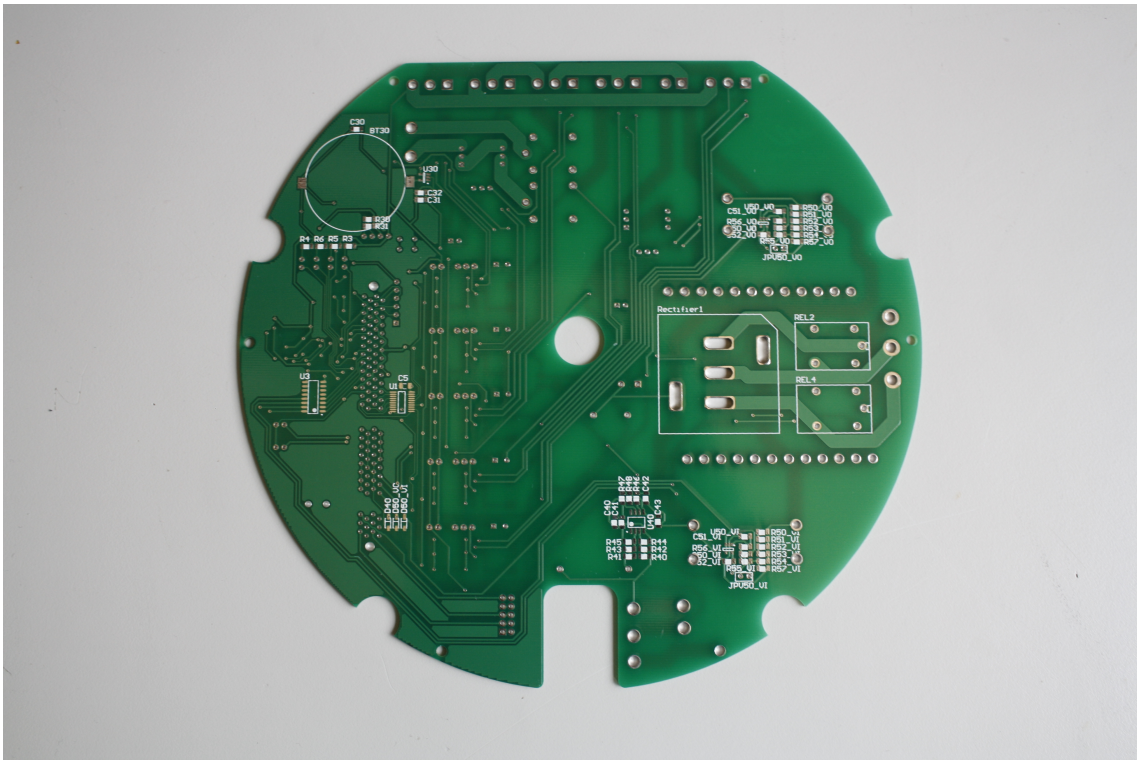

Figure A-2: Bottom Layer of the PCB

Figure A-3: Generator built by 'AZ Renovables'.

Figure A-4: Photo of the Generator coupled to a induction machine (wind turbine simulator).

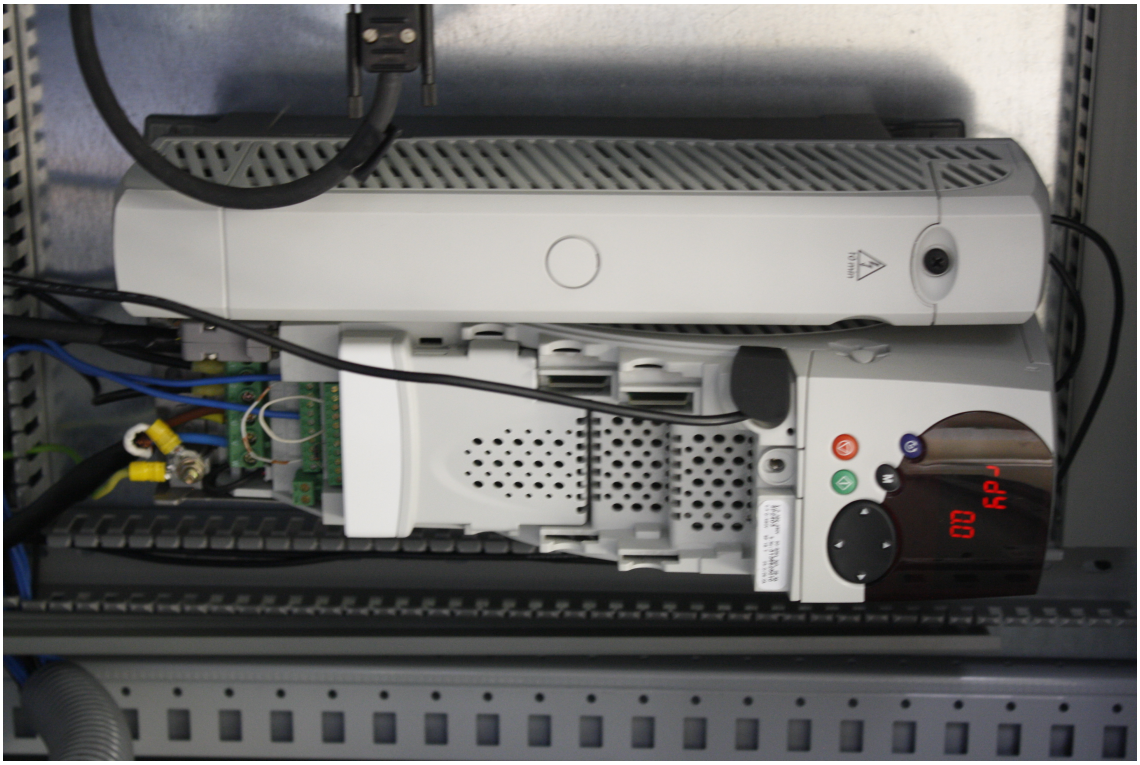

Figure A-5: Photo of the frequency converter used.

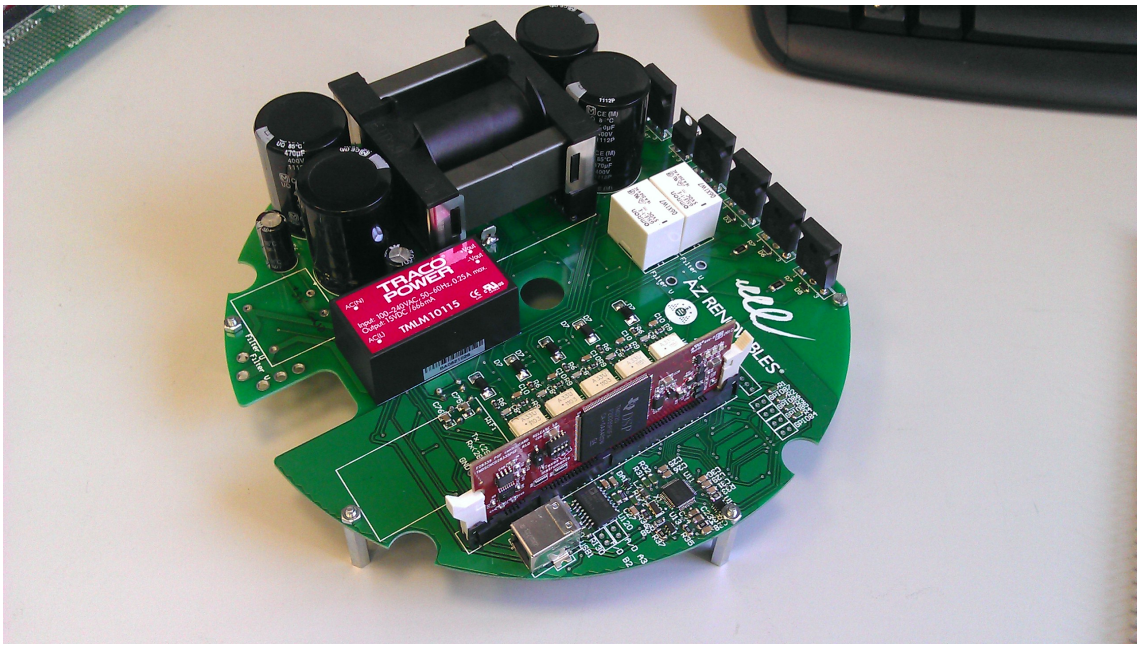

Figure A-6: Photo of a mounted PCB (DSP view).

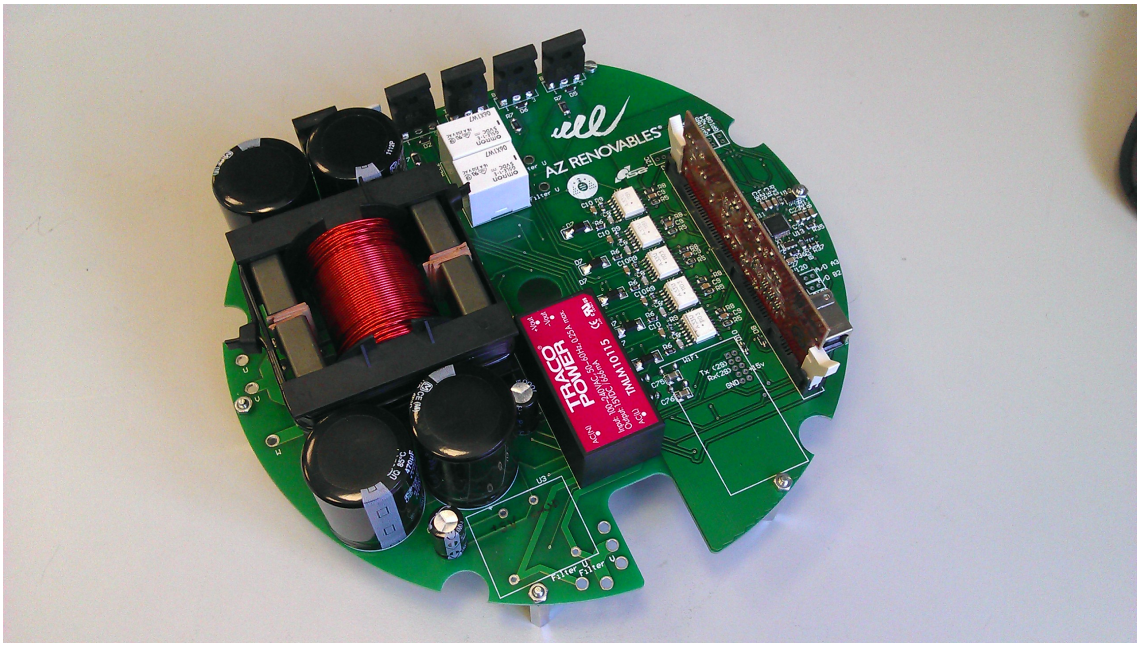

Figure A-7: Photo of a mounted PCB (coil view).

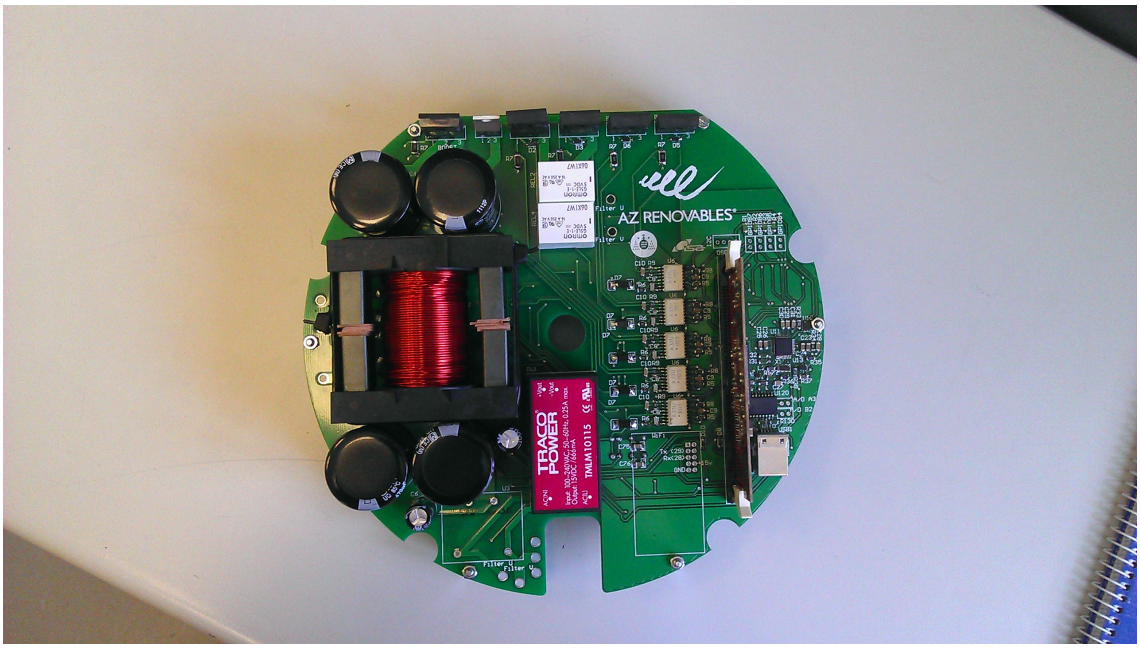

Figure A-8: Photo of a mounted PCB (top view).

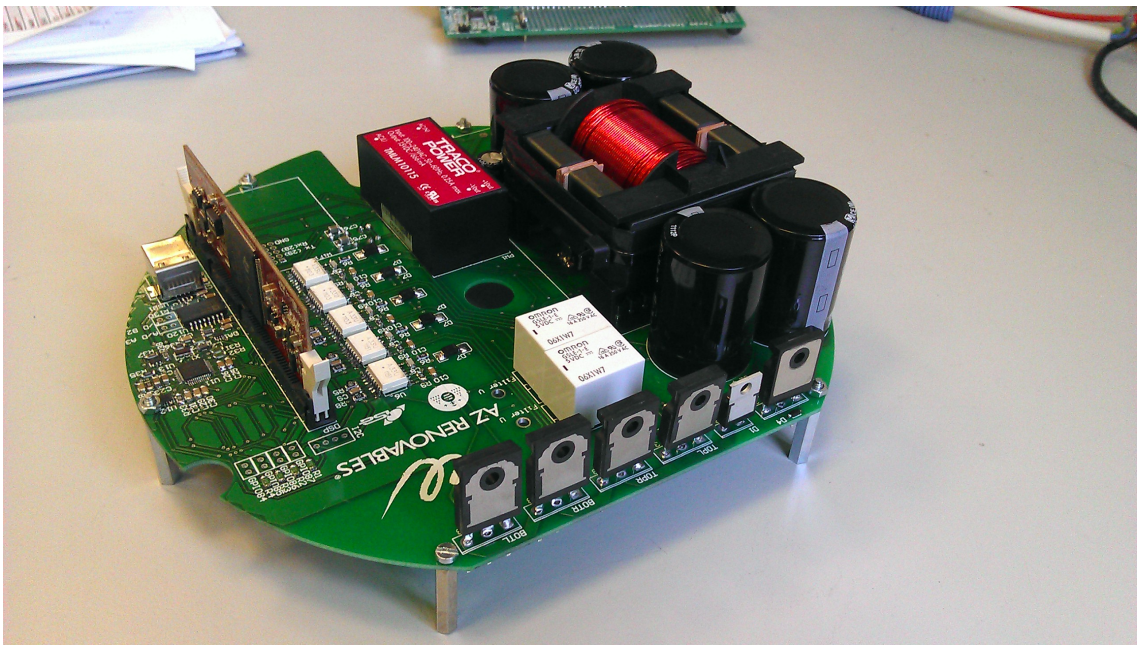

Figure A-9: Photo of a mounted PCB (IGBTs view).

Bibliography

[1] C. Lumbreras, Proyecto Fin de Carrera. Análisis y Diseño de un Sistema de Control Digital para Microgeneración Eólica. Universidad de Oviedo, 2011.

[2] A. E. (Arthur E. Fitzgerald, C. Kingsley, and S. D. Umans, Electric Machinery. McGraw-Hill, 2003.

[3] M. H. Rashid, Power Electronics: Circuits, Devices, and Applications. Pearson/Prentice Hall, 2004.

[4] Tony Burton et. al., (ed), Wind Energy Handbook , John Wiley and Sons 2001 ISBN 0 471 48997 2

[5] Betz, A. (1966) Introduction to the Theory of Flow Machines. (D. G. Randall, Trans.) Oxford: Pergamon Press.

[6] G. Son, H.-J. L. Lee, and J.-W. Park, "Estimation of Wind Turbine Rotor Power Coefficient Using RMP Model," in IEEE Industry Applications Society Annual Meeting, 2009. IAS 2009, 2009, pp. 1 –8.

[7] K. Mok, "Identification of the power coefficient of wind turbines," in IEEE Power Engineering Society General Meeting, 2005, 2005, pp. 2078 – 2082 Vol. 2.

[8] R. J. Wai, C. Y. Lin, and Y. R. Chang, "Novel maximum-power-extraction algorithm for PMSG wind generation system," IET Electric Power Applications, vol. 1, no. 2, pp. 275 –283, Mar. 2007.

[9] A. Monroy and L. Alvarez-Icaza, "Real-time identification of wind turbine rotor power coefficient," in 2006 45th IEEE Conference on Decision and Control, 2006, pp. 3690 –3695.

[10] Siegfried Heier, "Grid Integrationof Wind Energy Conversion Systems," John Wiley & Sons Ltd,1998, ISBN 0-471-97143-X

[11] S. M. Silva, B. M. Lopes, B. J. C. Filho, R. P. Campana, and W. C. Bosventura, "Performance evaluation of PLL algorithms for single-phase grid-connected systems," in Conference Record of the 2004 IEEE Industry Applications Conference, 2004. 39th IAS Annual Meeting, 2004, vol. 4, pp. 2259–2263 vol.4.

[12] M. Yoshida, Y. Hanashima, and T. Yokoyama, "1MHz sampling high-speed single-phase PLL control using FPGA based hardware controller," in Power Electronics and Motion Control Conference (IPEMC), 2012 7th International, 2012, vol. 1, pp. 620–625.

[13] Y. Xia, K. H. Ahmed, and B. W. Williams, "A New Maximum Power Point Tracking Technique for Permanent Magnet Synchronous Generator Based Wind Energy Conversion System," IEEE Transactions on Power Electronics, vol. 26, no. 12, pp. 3609 –3620, Dec. 2011.

[14] E. Koutroulis and K. Kalaitzakis, "Design of a maximum power tracking system for wind-energy-conversion applications," IEEE Transactions on Industrial Electronics, vol. 53, no. 2, pp. 486–494, April.

[15] I. Kortabarria, J. Andreu, I. Martínez de Alegría, E. Ibarra, and E. Robles, "Maximum power extraction algorithm for a small wind turbine," in Power Electronics and Motion Control Conference (EPE/PEMC), 2010 14th International, 2010, pp. T12–49 –T12–54.

[16] M. W. Uddin, M. Y. Sumon, R. Goswami, M. Asif, and K. M. Rahman, "Sensorless peak power point tracking system for small scale wind turbine generators,"

in Developments in Renewable Energy Technology (ICDRET), 2009 1st International Conference on the, 2009, pp. 1 –4.

[17] C. Patsios, A. Chaniotis, M. Rotas, and A. G. Kladas, "A comparison of maximum-power-point tracking control techniques for low-power variable-speed wind generators," in 8th International Symposium on Advanced Electromechanical Motion Systems Electric Drives Joint Symposium, 2009. ELECTROMOTION 2009, 2009, pp. 1 –6.

[18] IEEE Recommended Practices and Requirements for Harmonic Control in Electrical Power Systems," IEEE Std 519-1992 , vol., no., pp.0_1,, 1993 doi: 10.1109/IEEESTD.1993.114370